# Accepted Manuscript

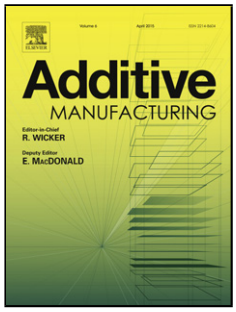


Title: Development of a Hot-Melt Extrusion (HME) process to produce drug loaded Affinisol™ 15LV filaments for Fused Filament Fabrication (FFF) 3D printing

Authors: Elke Prasad, Muhammad T. Islam, Daniel J. Goodwin, Andrew J. Megarry, Gavin W. Halbert, Alastair J. Florence, John Robertson

PII: S2214-8604(18)30787-5
DOI: https://doi.org/10.1016/j.addma.2019.06.027
Reference: ADDMA 776

To appear in:

Received date: 3 October 2018
Revised date: 12 June 2019
Accepted date: 30 June 2019

Please cite this article as: Prasad E, Islam MT, Goodwin DJ, Megarry AJ, Halbert GW, Florence AJ, Robertson J, Development of a Hot-Melt Extrusion (HME) process to produce drug loaded Affinisol™ 15LV filaments for Fused Filament Fabrication (FFF) 3D printing, *Additive Manufacturing* (2019), https://doi.org/10.1016/j.addma.2019.06.027

# Development of a Hot-Melt Extrusion (HME) process to produce drug loaded Affinisol™ 15LV filaments for Fused Filament Fabrication (FFF) 3D printing.

Elke Prasad[a], Muhammad T. Islam[a], Daniel J. Goodwin[b], Andrew J. Megarry[c], Gavin W. Halbert[a], Alastair J. Florence[a], John Robertson[a]*

[a] *EPSRC Future Manufacturing Research Hub in Continuous Manufacturing and Advanced Crystallisation, University of Strathclyde, Technology and Innovation Centre, 99 George Street, Glasgow, G1 1RD, UK.*

[b] *GSK Research and Development, Park Road, Ware, Hertfordshire SG12 0DP, UK.*

[c] *Pharmaceutical Technology and Development, AstraZeneca, Pepparedsleden 1, SE 431 83, Mölndal, Sweden*

*Corresponding Author:

Dr John Robertson, Phone: +44(0)1414447130; E-mail: j.robertson@strath.ac.uk.

**Abstract**

The aim of the present work was to develop a pilot scale process to produce drug-loaded filaments for 3D printing of oral solid dose forms by fused filament fabrication (FFF). Using hot melt extrusion, a viable operating space and understanding of processing limits were established using a hydrophilic polymer (hydroxypropyl methylcellulose (HPMC) - Affinisol™ LV15). This was then extended to formulate paracetamol (PCM) loaded Affinisol™ 15LV filaments across a wide range of compositions (5 - 50 wt% drug). From the process development work, challenges in achieving a pilot scale process for filament production for pharmaceutical applications have been highlighted. 3D printing trials across the range of compositions demonstrated limitations concerning the ability to print successfully across all compositions. Results from characterisation techniques including thermal and mechanical testing when applied to the formulated filaments indicated that these techniques are a useful predictive measure for assessing the ability to print a given formulation via filament methods. Oral solid dosage forms of variable surface area to mass ratios printed from suitable filament

compositions demonstrated the ability to modify the release rates of drug for fixed formulations across substantial timescales.

Keywords: Fused filament fabrication (FFF); Hot Melt Extrusion; Oral solid dosage form; hydroxypropyl methylcellulose (HPMC); modified release paracetamol

## 1 Introduction

Hot Melt Extrusion (HME) has been traditionally used as a processing platform for the plastics industry since the early stages of polymer processing in the 1930's. Research and development within the last 2 to 3 decades has enabled HME to be utilised as a viable platform for pharmaceutical applications and has resulted in a number of HME processed products reaching the market [1]. HME has proven to be a robust method for producing oral drug delivery systems, particularly by enhancing solubility and bioavailability of poorly water soluble active pharmaceutical ingredients (API) [2]. HME has also successfully been used to produce sustained and controlled release oral solid dosage forms (OSD) [3]. In recent years, researchers have started exploring HME to prepare drug-loaded filaments for use in three-dimensional (3D) printing to prepare pharmaceutical oral solid dosage forms with customisable properties [4-7].

There are a variety of 3D printing technologies available, including stereolithographic, powder bed based, selective laser sintering, fused filament fabrication, semi-solid extrusion and powder bed inkjet printing [8]. Fused filament fabrication (FFF) 3D printing has received notable interest in recent years for preparation of OSD utilising drug loaded polymer filaments. FFF shows advantages because of its lower costs, ability to print multiple polymers/formulations in a single structure and the capacity to create highly structured dose forms e.g. hollow and porous objects with the potential to customise release characteristics and generate personalised medicines [9, 10].

A number of early research approaches for FFF 3D printing used commercially available filament, such as PVA, PLA and acrylonitrile butadiene styrene (ABS) filaments [11]. The filaments were typically immersed for 24 hours in an API – organic solvent solution to impregnate and load the drug into the filament. For example, commercial PVA filaments were soaked in an ethanol solution of fluorescein [12], saturated solution of prednisolone in methanol [13], ethanol solution of 4-ASA or 5-ASA [14]. The resulting filaments were oven dried prior to processing using a desktop FFF 3D printer. This method of immersing filaments in a solution to load the drug is time consuming and required further processing such as drying

prior to extrusion using a FFF 3D printer for fabricating tablets. This method results in limited or low API loadings (~1 - 2 wt%) in the filament.

To avoid the required time, overcome the pre-processing of the filaments and achieve higher drug loadings in the filaments, hot-melt extrusion of the pre-blended powder with API has been reported by recent workers in this area to produce filaments for FFF 3D printing. Examples of this include Goyanes et al., who extruded a filament from a physical blend of PVA powder with budesonide and paracetamol using a very basic single screw filament extruder made by Noztek and Filabot respectively [14, 15]. Other workers have used small bench-top twin screw extruders HAAKE miniCTW, HAAKE mini lab and Pharma 11 to produce filaments using PVP with theophylline or dipyridamole [16], PLA with acetaminophen and furosemide [11, 17], eudragit and HPC with theophylline [18]. Through the use of these types of twin-screw extruders higher drug loadings of up to 30 wt% [19] have been achieved and reduced the time to prepare filaments.

Commercial FFF 3D printers generally require a filament with specific physical dimensions (generally 1.75 ± 0.05 mm is a typical printer manufacturer specification) to enable smooth operation of the printer. Although the authors [14-18] reported filaments produced by these bench-top scale extruders were within the diameter required for 3D printing, the effect of processing parameters such as screw speed, feed rate and die temperature in filament fabrication has not been explored or reported. It can also be inferred from the equipment scale that only small lengths of filament may have been produced.

From this early work on FFF for OSD manufacture, it is clear that preparation of drug loaded filaments suitable for FFF 3D printing remains a challenge. For example, die swell of the extrudates as it exits the HME has a significant impact on filament diameter. Researchers such as Carneiro et al., have reported that several trials are required to achieve suitable filament diameter [20]. Additionally, the physical character of the filament such as brittle, plastic, stiffness and strength need to be sufficient to prevent filament breakage and enable the printer to operate. For example, Zhang et al., have reported this and recognised the need to assess the filament suitability for printing and have reported requirements to mechanically modify 3D Printers to compensate for fragile filaments [19].

In this study, a pilot scale twin-screw extruder was used to manufacture filaments (up to 100 m in length) and explore the effect of processing parameters of the HME during filament fabrication. Formulation and manufacturing of filaments at this scale has not previously been reported and limited detail around HME processing conditions to enable sufficient quantities of filament to support development such as clinical testing have not been reported. In this study a hydroxypropyl methylcellulose (HPMC) based polymer Affinisol™ 15LV was used as a carrier and Paracetamol was used as a model API to produce filaments for FFF 3D printing. Affinisol™ has been combined at a 1:1 ratio with Kollidon® VA64 with low drug loadings at laboratory scale [21]. The challenging processing properties of Affinisol™ during HME have been highlighted [22] and this is the first reported instance of Affinisol™15LV alone being used

for formulation of a drug loaded filament across a wide range of high API loadings at pilot scale.

Affinisol™ 15LV was selected as the polymer based upon-

1) Wide use of HPMC in pharmaceutical dosage forms for both immediate-release and modified release formulations.
2) HPMC is known to stabilize amorphous systems which often result from HME.
3) HPMC is generally a challenging class of polymer for HME. This is due to its broad range of glass transition temperature (160 °C – 210 °C), low degradation temperature and high melt viscosity makes it challenging to process via HME and often requires addition of a plasticizer to improve the processability of HPMC via HME but with consequences in crystallization of the drug during storage due to other additives [23].
4) Affinisol™ 15LV however is a modified HPMC polymer introduced by Dow Chemical Company, specifically developed to use in HME applications which provides a lower glass transition (Tg) temperature (117 °C – 128 °C) and a lower melt viscosity than presently available grades of HPMC and is claimed to be suitable for HME between 150 °C to 205 °C, avoiding the requirement for plasticizer [24, 25].

Based on these premises, the key aims of the present work were:

1) To explore the range of viable HME operating parameters for Affinisol™ 15LV using a 16 mm pilot scale twin-screw extruder.
2) To develop operating parameters to produce filaments 100 m in length using the same polymer for FFF 3D printing.
3) Assess the effect of HME processing parameters (extruder screw speed, die zone temperature and feed rate) and die geometry to develop methods to control the resulting filament diameter
4) To produce 100 m long filaments with a wide range of API content (0 - 50 wt%), assess the properties of these filaments and convert into OSD via 3D FFF printing.
5) To produce 3DP dose forms with a range of structures and assess the impact on dissolution.

## 2 Materials and methods

### 2.1 *Materials*

Hydroxypropyl methylcellulose (HPMC), grade Affinisol™ 15LV HME, a water soluble, amorphous polymer with a molecular weight of less than 100kDa, bulk density of 0.42 kg/l and D(0,5) of 104.49 µm, was kindly donated by the Dow Chemical Company ("Dow"). Paracetamol powder (PCM) grade Form I, D(0.5) of 52.6µm was purchased from Mallinckrodt Inc., USA. All chemicals were used as received.

## *2.2 Methods*

### *2.2.1 Blending*

Binary mixtures of drug containing 5 – 50 wt% PCM were blended with polymer (Affinisol™ 15LV) by weighing out the samples on an analytical balance and blended using a bin blender (AgiBlend MB015AB Blender, Pharmatech, Warwickshire, UK) with a 1 L vessel. The materials for each formulation were blended for 20 minutes at a set blend speed and agitation speed of 30 rpm and 700 rpm, respectively.

### *2.2.2 Hot-Melt Extrusion*

HME was carried out using a Eurolab 16, a 16 mm co-rotating twin-screw extruder (Thermo Fisher Scientific, Karlsruhe, Germany). The length of the screw in relation to the barrel diameter (L/D ratio) is 40:1 and the extruder consists of a barrel (10 zones) along with a die zone. The feeder (Gravimetric Flexwall Dosierer, Brabender Technology, Duisburg, Germany) fed into zone 1 through a feed funnel and the co-rotating screws carry forward the materials towards the die end. The screw configuration of the shaft used is shown in Figure 1. It was configured with two mixing blocks consisting of mixing elements at 30°, 60° and 90°. The twin-screw extruder can heat up to maximum 300 °C during hot-melt extrusion and can extrude the materials at maximum 1000 rpm screw speed. Machine data motor power, torque, pressure and temperatures were logged using PharmaMV software (Perceptive Engineering Ltd., Daresbury, Cheshire, UK).

### *2.2.3 Method development to prepare filaments for FFF 3D printing*

Filaments for 3D printing were prepared via HME using Eurolab 16 twin-screw extruder. Affinisol™ 15LV was extruded to produce filaments via round extruder dies with diameters of 1.0, 1.5, 1.6 and 3.0 mm. The 1.0 and 3.0 mm die were supplied by Thermo Fisher and the 1.5 and 1.6 mm were made in-house. The filaments were cooled and conveyed by an Air Cooled Conveyor 1200 (Thermo Scientific, Karlsruhe, Germany) with available speed range from 1 – 10 on a nominal analogue scaling. Upon exiting the conveyor, the filaments fell through a fixed drop of 1.2 m and gathered in a 600 mm diameter drum. The filaments have a natural tendency to form a loose coil. After processing, the filaments were stored in a sample bag. The filament diameter was measured at line using an ID-C X series digimatic indicator (accuracy: 0.001 mm, Mitutoyo Absolute, Japan). A minimum of 10 samples were measured.

### *2.2.4 Mechanical Testing*

Mechanical properties of filaments were tested on a Texture Analyser TA-XT (Stable Micro Systems, Godalming, UK) equipped with a mini 3-point bend rig (Figure 2) . Filaments samples were cut to a length of 2cm. Digital callipers (Axminster.co.uk, 0.01mm) were used to measure the length and diameter of the samples, which were placed centrally on the two lower support beams with a gap of 0.8 cm. The upper blade speed was set to 0.5 mm/sec until a trigger force of 0.049 N was achieved. Testing was conducted with a blade speed of 0.02 mm/sec and a total displacement of 4.5 mm. Data acquisition and analysis was performed with Exponent software (version 6.1.11.0) with a rate of 25 points per second. Five replicates

were tested for each sample. Stress-strain graphs were plotted based on the following relationships for stress and strain:

$\sigma_f = \frac{FL}{\pi R^3}$ (circular cross section) (Equation 1)

Where
$\sigma_f$ is the flexural-stress.
F is the applied force in Newtons.
L is the span (or gap) in millimetres.
R is the radius of the specimen in millimetres.

$\varepsilon_f = \frac{600\ s\ h}{L^2}$ % (Equation 2)

Where
$\varepsilon_f$ is the flexural strain (expressed as percentage)
s is the deflection in millimetres
h is the thickness of the test specimen in millimetres
L is the span (or gap) in millimetres

The flexural modulus was determined as the slope of the linear region of the stress strain graph between 1.5 and 5 % strain. Maximum stress and associated strain values were also derived from the obtained stress strain graphs.

### *2.2.5 Differential Scanning Calorimetry*

Differential Scanning Calorimetry was performed on a Netzsch Polyma DSC 214. 5 mg of pelletised sample was accurately weighed into a 25 µL aluminium pan with pierced lid and crimped. Samples were analysed in triplicate and exposed to heat/cool/heat cycles in a helium atmosphere (40 mL/min) from 0 to 190 ˚C at a heating rate of 20 ˚C/min. Empty aluminium pan were used as reference and blank. Prior to analysis, 5, 10, 20, 30, 40, 50 wt% PCM samples had been stored for 1 year at 25 ˚C and 60 % RH. 25, 35, 45 wt% PCM samples had been stored 5 months under the same conditions. It was noted that changes in the filament character (solidification, and appearance of crystalline material in higher concentrations) occurred within a short timescale post extrusion. Therefore, materials were stored to ensure an endpoint. Additionally, DSC analysis was based on all three cycles and analysed for thermal events. Aging effects of samples were erased in the first heating cycle.

### *2.2.6 X-Ray Diffraction (XRD)*

XRD methods were used to assess the crystalline state of the PCM in the physical mixtures, extrudates, and 3DP tablets at room temperature. The apparatus was a Bruker D2 Phaser 2nd Gen benchtop diffractometer operating in Bragg-Brentano (theta–theta) flat plate geometry, using a Cu anode at 30 kV and 10 mA, emitting $K\alpha_{1,2}$ radiation with a wavelength of 1.5406 Å with a 0.6mm anti divergence slit. A 10.5 mm Ni low-Beta filter was employed with 2.5° Soller

slits and a LynxEye 1D Position Sensitive Detector with a 5.83° opening. The samples were rotated at 15 rpm to minimise any preferred orientation effects. The samples were scanned from 5 to 35° 2Θ with a step size of 0.01° and a counting time of 0.1 s per step.

### *2.2.7 3D printing of the dosage forms*

All 3D printed tablets were printed using a filament printer which had been assembled in house. The basic printer was a STARTT printer kit from iMakr. UK. The separate extruder filament feed to the hot end via a Bowden system was removed and replaced by an integrated Mk8 Makerbot filament feed-extruder-hot end. This was done to avoid using a Bowden system to minimise the stresses placed on the filament during printing. The printer bed was a non-heated system and printing was direct onto print plates supplied by iMakr. The non-heated build volume was 120 x 140 x 130 mm (W/D/H) and the nozzle diameter was 0.4 mm.

The tablets were designed in SOLIDWORKS© 2017 to have a weight of 200 mg based on a the density of PLA (poly lactic acid density = 1.25 kg/cm$^3$[26]) and then saved as a stereolithographic file format (.stl). This file format was then converted into a G-code (.gcode) format using CURA v2.5, allowing upload of file to the printer. Each tablet was printed at 190 ˚C at a print speed of 40 mm/s with a layer height of 0.2 mm and 100 % infill. This infill was chosen so that the surface to volume relationship and structure of the printed dose forms was a function of the CAD design. Four different tablet shapes were created: solid cylinder (SC), slotted grid (SLG), slotted grid with cap (SLGC) and slotted grid extended (SLGE) (Figure 3). Tablet dimensions were measured using digital callipers (Axminster.co.uk, 0.01 mm) and tablet weights measured using a 1DP analytical balance.

### *2.2.8 Content analysis of extrudates*

Content analysis was performed using a UV-Vis spectrophotometer (ALS SP7000, Wokingham, UK). Pelletised (1 mm) extrudates were dissolved overnight in phosphate buffer pH 5.8 (EP). Analysis was performed by UV-Vis analysis equipped with a flow cell cuvette with a 1 mm path length. The system was flushed with a minimum of 20 mL of sample solution (at 20 mL/min) prior to analysis. The drug content of samples was calculated based on the UV absorbance at 243 nm and the response factor (RF) of PCM standards.

### *2.2.9 Drug release studies*

Dissolution studies were carried out in a USP type II dissolution apparatus (Automated Lab Systems, Wokingham, UK) in 1000 mL of phosphate buffer pH 5.8 (EP) at 37 ± 0.5 ˚C and 50 rpm. Tablet sinkers were used for 3DP tablets. Drug release was measured at 5 min intervals for the first 20 minutes and 20 minute intervals thereafter for a total of 12 h. Analysis was performed by UV-Vis analysis equipped with 1 mm (50 wt% PCM formulations) or 10 mm (10 wt% PCM formulations) path length flow cell cuvettes. Flow cell cuvettes were flushed with a minimum of 20 mL buffer (at 20 mL/min) prior to analysis. Absorbance (243 nm) of samples was measured using a UV-Vis spectrophotometer (ALS SP7000, Wokingham, UK). The system was operated in a closed loop configuration.

## 3 Results and Discussion

### *3.1 Initial screening of HME operating conditions for Affinisol™ 15LV*

An initial assessment of the viable processing conditions for Affinisol™ 15LV by HME was made with the Eurolab 16, equipped with a fixed screw geometry and a round, 3.0 mm diameter die. A fixed feed rate of 1.0 kg/h was used. Barrel temperatures of 150 °C, 180 °C and 210 °C were selected, based on the manufacturer's recommended processing temperature for Affinisol™ 15LV of approximately 150 °C – 205 °C. Extrusion was carried out across a screw speed range of 100 – 1000 rpm to assess the impact of processing temperature and screw speed to identify any equipment limits due to over-torque and over-pressure (entering a shutdown state at maximum 24 Nm and 100 bar) as well as impact on the quality of the resulting filaments. To assess quality of the filaments, extruded filament strands were visually assessed for colour and clarity, as well as physical faults such as surface faults, strand texture and bubbles (Figure 4).

The lowest barrel temperature of 150 °C and lower screw speeds of 100 and 200 rpm caused the equipment to stall because of the torque exceeding 24 Nm (Figure 5). The associated pressure was circa 34 bar. Increasing the screw speed above 200 rpm resulted in a reduction in torque and pressure. This is due to shear thinning behaviour of the polymer from the increased screw speed. However, as the screw speed increased above 500 rpm, the polymer extrudate became darker and increased signs of degradation were visible (Figure 4).

An increase in barrel temperature to 180 °C and 210 °C respectively also resulted in a drop in torque and pressure values due to the reduction in the polymer viscosity. Similar to the behaviour at 150 °C, as the screw speed increased, an overall drop in the torque and pressure was observed. At speeds above 400 rpm for the 180 °C and above 200 rpm for the 210 °C, the extrudate became discoloured and at 500 rpm and above was deemed unacceptable. In all cases as the screw speed increased, a greater degree of bubbles and foam like nature was observed for the extrudates. Based on these observations, degradation of Affinisol™ 15LV was influenced by a combination of thermal and shear stress effects. Similar effects of heat and shear on polymer degradation have been reported for a range of other polymeric materials [27]. As a result of these observations and the melting point of PCM being 169 - 171 °C a maximum barrel temperature of 180 °C and maximum screw speed of 500 rpm was used for the remainder of the study.

### *3.2 Method development to prepare Affinisol™ 15LV filaments of suitable dimensions for FFF 3D printing*

During the extrusion of Affinisol™ 15LV, a number of factors can affect the diameter of the resulting filaments. For example, die diameter and degree of swelling of the polymer strand as it exits the die, processing conditions such as temperature, feed rate and screw speed as well as downstream equipment altering the tension/stretching experienced by the filament as it is extruded.

Therefore, an initial set of experiments using a 1mm, 1.5mm and 3mm round die at 180 °C extrusion temperature, 1 kg/h mass flow across a screw speed of 100-500rpm were carried out to assess the impact on filament dimensions. The speed of the downstream air-cooled filament conveyor was also varied across its working range to assess if there was any impact (such as varying tension on the extruded filament).

The results of filament diameter, conveyor belt speed and screw speed for these extrusions are plotted in Figure 6. As a reference target, the target diameter (1.75mm ± 0.05 mm) of a commercially available PLA filament (ex CEL ROBOX, UK) is also shown.

Figure 6 shows that the diameter of all the resulting filaments is not substantially affected by the speed of the downstream conveyor. This is most likely due to the conveyor belt in this case being coated in a low friction material and hence there is little friction to stretch or compress the filament and affect diameter. Additionally, it is likely that as the filament fell through a fixed drop as it exited the conveyor that this was the over-riding effect

In all cases, the diameter of the resulting filament is notably larger than the dimensions of the die. The filament dimension also increases with screw speed. This is due to die swell the degree of which was impacted by the nature of the polymer and rheological changes in the polymer resulting from shear in the system. Aho et. al., discusses this phenomenon in detail and summarises that the higher shear (e.g. higher screw speed) the greater the degree of die swell [28].

Figure 7 shows the response of screw torque and die pressure from the twin-screw extruder during the above experiments. Die pressure and screw torque both decrease because of increased screw speed. This is due to higher shear resulting in a drop in viscosity of the melt. For the 1.0 and 1.5mm (where the resistance to flow through the die is greater), there are lower limits to the operable screw speed due to maximum torque of 24 Nm and maximum pressure of 100 bar being exceeded. Hence, filaments could not be formed below 200 rpm for the 1.5 mm die and below 400 rpm for the 1mm die at the flowrate of 1 kg/h.

From this exercise, the closest filament dimension (1.89 ± 0.02 mm) to the target (1.75 ± 0.05mm) was achieved using 1.5 mm extruder die at 200 rpm. From the above results, a reduction in screw speed could reduce this diameter and perhaps meet the target.

However, from the torque vs speed data gathered, the extruder is close to a stall over-torque condition at 1 kg/h flowrate. Experiments were conducted at screw speeds between 150 and 200 rpm but resulted in too high a torque to give a satisfactory process. Therefore, to allow processing at lower speeds, the flowrate was reduced to 0.75 kg/h to allow further work with the 1.5 mm extruder die and further develop the method to produce filaments. As the conveyor speed did not substantially affect the diameter of the filaments a conveyor speed setting of 5 was selected for the remaining work.

Table 1 shows the results of filament diameter at a flow rate of 0.75 kg/h for screw speeds of 50-200 rpm and 1.5mm die. The results obtained for 200rpm and below at 1 kg/h for the 1.5mm die are also included in Table 1 for comparison.

From these results, it can be seen that at the screw speed of 200 rpm, the filament diameter appears unchanged with changes in flowrate but as the screw speed is further reduced, the degree of die swell is reduced in line with the previous experiments and at 50rpm, the target filament dimensions are met.

From this exercise, it is clear that for a fixed extrusion temperature a balance between screw speed, die dimension and mass flowrate must be met in order to produce a filament of suitable dimensions. It is also clear that the overall operating range in which this can be achieved is relatively narrow compared with the equipment capability.

These learnings were then used as a basis to develop methods to produce filaments (dia. 1.75mm ± 0.05mm) for FFF 3DP across a wide range of API concentrations.

### *3.3 Method development to prepare API loaded Affinisol™ 15LV filaments of suitable dimensions for FFF 3D printing*

Paracetamol, as a model drug substance, was included in the feedstock to produce drug-loaded filament ranging from 5 - 50 wt% API content.

The inclusion of API caused a significant drop in the viscosity of the mixture compared with the pure polymer. The drop in viscosity increases as the API loading increases and was due to the plasticising effect of the API. This also resulted in a reduction in filament diameter, therefore the die size was increased slightly from 1.5 mm to 1.6 mm to help compensate. It was evident that this reduction in viscosity with introduction of API would need to be addressed in order to produce both a filament of suitable dimensions but also a filament with sufficient viscosity to be able to support itself post extrusion across the wide range of compositions targeted. No further reduction in screw speed was possible (50 rpm is the lowest possible for this machine). It has been reported that viscosity of polymer systems decreases with increased temperature [22]. Therefore, the die temperature was adjusted inversely with the API loading to compensate shifts in viscosity and target the suitable filament dimensions. Table 2 shows the results of filament diameters achieved at the die temperatures applied for key compositions. Figure 8 shows images of the filaments made at all compositions, Figure 9 show the results of suitable die temperatures used to produce filaments with the target diameter.

Extruded filaments containing 5 to 20 wt% PCM were opaque/clear in appearance and relatively stiff (Figure 8). From 25 to 35 wt% PCM, filaments had a similar visual appearance but were much softer. Filaments with 40 to 50 wt% PCM content were white in appearance, relatively stiff with a smooth surface. As API loading increased, the degree of internal bubbles decreased. Overall, it appeared that three basic types of filament were being formed. Up to circa 20 wt% concentration a polymer rich, stiff strong filament that is modestly plasticised.

Between 25 - 35 wt%, a filament that is supersaturated but still largely amorphous in character. Above 40 wt%, heavily supersaturated with onset of free crystalline material. The subsequent analysis, in particularly the mechanical testing, DSC and XRD aligns this observation from the extrusion. Figure 10 presents the die swell ratio data for the range of compositions and die temperatures used. The transition between 30 and 40 wt% at 130°C shows a dramatic shift coinciding with the presence of crystals in the system. A similar observation was cited by Aho et al and was attributed to the presence of solid fillers decreasing the elasticity ratio between the normal force and shear stress. Increasing particle concentration reduced die swell during extrusion [29].

In a similar theme, the overall trend in motor torque data agreed with the visual appearance and stiffness of nature of extruded filaments across the range of formulations. With increasing API concentrations in the formulation, a decrease in recorded torque values was observed from 22 Nm for Affinisol™ 15LV to the lowest torque value of 8 Nm for the 30 wt% PCM formulation as the materials was being plasticised (Figure 11). Further increase in API concentration to 40 wt% and 50 wt% PCM saw a modest rise in torque; this is most likely due to the presence of particulate PCM at the higher loadings. Die pressure dropped marginally from pure Affinisol™ 15LV to 30 % drug loading and then rose sharply as the drug loading increased to 50 wt% (Figure 11). This is likely to be due to the presence of particulate PCM at the die at the high API loadings increasing resistance to flow.

### *3.4 3-point bend test measurements on extruded filaments.*

In the HME - FFF 3D printing process stream, the extruded filament is subsequently fed into the FFF 3D printer. Within the printer, a feeding gear conveys the filament. To convey the filament successfully within the printer, the filament is required to withstand forces applied by the feed gear and during the conveying process. In addition, the filament may be required to follow a convoluted path from the feed gear to the print nozzle exerting additional forces on the filament. Brittle filaments may break, whereas the feed gear may be unable to convey the filament if the filament is very pliable. Zhang et al has previously reported on mechanical properties of FFF filaments causing problems during 3D printing. Specifically, brittle filaments breaking due to stresses applied by the feeding gear and soft filaments pushed aside by the feeding gear [19].

With the purpose of establishing a screening tool for identifying the printability of extruded filaments, a test to assess the mechanical properties of extruded filaments was developed. From this work, three basic groups of mechanical properties were identified. The results are shown in (Figure 12)

The first group of materials were in the concentration range of 5 - 20 wt% PCM, showed a defined linear (elastic) region at low strain values.

The lowest concentration of PCM (5 wt%) was the stiffest and strongest filament, with the highest flexural modulus of 4.4 MPa and the highest maximum stress of 45.1 MPa

(supplementary data, Figure S 1). With an increase in PCM (10 and 20 wt%) concentration, the flexural modulus only decreased slightly to 3.3 and 3.1 MPa, respectively. The maximum stress decreased similarly to 32.3 and 31.9 MPa. All filaments exhibited elastic behaviour at low strain values, followed by yielding behaviour with subsequent plastic deformation. At these low PCM concentrations, the majority of the system is composed of long polymer chains allowing movement (yielding), but still maintain sufficient polymer-polymer interactions to remain intact (not break). The mechanical properties of these filaments were dominated by properties of the polymer, which is plasticised with increasing concentrations of PCM. This is in line with the DSC analysis of these filaments, showing increasing plasticisation resulting in decreasing Tg with increasing PCM concentration. All of these filaments were printable.

The second group of materials, at medium PCM concentrations (25, 30, 35, 40 and 45 wt%), showed a significant change in the mechanical behaviour.

A large decrease in flexural modulus and maximum flexural stress was observed (e.g. for 35wt% these values were as low as 0.2 MPa and 3.6 MPa respectively). These filaments were softer and showed increased flexibility compared to low PCM concentration formulations. The mechanical properties at low strain values of these filaments were dominated by plastic behaviour rather than elastic behaviour, seen as a less well-defined linear relationship of stress and strain. A slight bend in the stress strain curve was observed around 12 – 20 % strain, which is in agreement with the observation of a faint lower yield point for low PCM concentration formulations. The significant change in mechanical properties is possibly due to PCM reaching a critical concentration to plasticize the system by reducing polymer-polymer interactions and therefore enabling increased movement of polymer strands. Although the planar benzene structure of PCM confers some steric restrictions, the overall small size of the PCM (Mw = 151 g/mol) molecule should enable the molecule to insert easily between polymer strands. DSC analysis of these filaments showed similar Tg temperatures around 30 ˚C, irrespective of drug loading of these formulations. The mechanical properties of these formulations were representative of a fully plasticized polymer system. This observation also coincided with the feeding gear of the FFF 3D printer failing to convey these filaments in the printer, as it was too soft.

The third group of materials at the highest (50 wt%). PCM concentration had a similar elastic behaviour (flexural modulus 3.8 MPa) at low strain values to the 5 – 20 wt% PCM concentrations. At higher strain values, it exhibited brittle failure seen as a sharp drop in stress at ~30 % strain.

This is due to PCM exceeding its solubility in the polymer system and a substantial content of free crystalline PCM regions in the filament, seen by the white appearance of the filament (Figure 8). The powder X-ray diffraction analysis of this filament showed an indication of crystallinity seen as a small peak at $2\theta$ = 24.1 (Figure 13), this finding was corroborated by the DCS analysis data showing a melting event at 160.3 ˚C (Figure 16). This filament was suitable for printing. While the 40 – 35 wt% showed some signs of crystalline content (observed by

DSC and visual observation of the filament) it was insufficient to render the filament stiff and strong enough for printing.

Overall, these results show that this type of screening tool was useful in establishing suitability for 3D printing and filaments need to have a substantial flexural modulus to enable printing. It also shows that it may not be possible to print across a continuum of concentrations due to excessive plasticisation or insufficient free crystalline material.

Other workers have reported 3-point bend testing tools for assessment of filaments for 3D printing. Zhang et al [19] and Verstraete et al [30] reported the maximum stress at break and the elongation at break only, but not the flexural modulus. As the maximum stress was not necessarily within the elastic region as shown above and differences in the specific method, direct comparison of results conducted with some caution.

### *3.5 X-ray diffraction (XRD)*

X-ray diffraction data of PCM powder showed sharp diffraction peaks characteristic of PCM form I, with the four main peaks seen at 2θ of 15.5, 18.1, 23.3 and 24.7 (Figure 13) [31].

As expected, the XRD pattern for Affinisol™ 15LV, an amorphous polymer (Mw < 100 kDa) without any long range molecular order, showed no indication of crystalline regions. Instead, two amorphous halos with low intensity were observed at 2-theta ~8 and ~19.

Diffraction peaks characteristic for crystalline PCM in terms of 2-theta position were seen in physical mixtures of PCM and Affinisol™ 15LV (Figure 13). The diffraction peaks only varied in intensity due to dilution effects as the PCM : AFF ratio was altered. Diffraction peaks were observed in 50 wt% PCM pelletised filaments showing some crystallinity. For concentrations 20 wt% and below, the XRD indicates that the filaments were all amorphous. (Figure 13). Freshly printed tablets were similar to that of Affinisol™ 15LV only i.e. largely amorphous. At 50 wt% PCM concentration, there was some minor diffraction peaks on top of the amorphous halo showing that the crystallinity was practically eliminated because of the printing process (Figure 14). This was in line with the visual glassy appearance of freshly printed tablets as well as the thermal analysis

A very small peak at 2θ = 31.09 was present in the Affinisol™ 15LV XRD pattern as well as the patterns for 3D printed tablets (Figure 14). However, this peak was not present at higher PCM concentrations. This peak corresponds to NaCl, which is a known impurity in Affinisol™ 15LV. This peak was seen by Gupta et al [24] but they did not assign it. This peak is not visible in the higher PCM concentrations due to the reduced concentration of Affinisol™ 15LV in the sample and hence reduced amount of impurity.

### *3.6 Differential scanning calorimetry (DSC)*

Samples were subject to a heat-cool-heat cycle during DSC analysis. In the first heating cycle, the thermal properties of the samples were assessed, aiming to identify the structure of the present polymer-API systems. Particular interest was paid to the miscibility of API and

polymer typically seen as a single Tg [21], [32] and the presence of crystalline material seen as melting endotherms. Additionally, PCM is a glass forming ability, GFA class 2 system, i.e. it crystallises upon heating from its amorphous state [33]. The Tg data from this analysis is shown in Figure 15. The DSC traces for the 50 wt% filament and printed tablet are shown in Figure 16 and Figure 17. The remaining DSC thermograms are shown in supplementary data (Figure S 3 to Figure S 5).

For the first heating cycle, crystalline PCM powder showed a sharp endothermic melting peak with an onset of 169.0 ˚C and a peak of 171 – 172 ˚C, indicative of PCM form I [34]. Processed Affinisol™ 15 LV did not show a clear Tg, instead a broad endotherm with minima around 50-60 ˚C and 105 ˚C were observed. Pelletised extrudates with 5 wt% and 10 wt% PCM only showed a single Tg with enthalpy relaxation at 54.6 ˚C and 51.9 ˚C, respectively, indicative of an amorphous, miscible API-polymer system [21]. At 20 wt% PCM, a Tg at 49.7 ˚C was recorded but also a melting endotherm peak at 139.7 ˚C, indicating the presence of two phases, amorphous PCM-polymer and crystalline PCM, in the sample. No obvious Tg was observed for formulations containing concentrations between 25 wt% and 40 wt% PCM, instead the presence of crystalline material was seen as melting endotherms. The endotherm melting peak temperature increased with increasing PCM concentrations from 139.7C at 20 wt% PCM to 160.3 ˚C (PCM form II) at 50 wt% PCM (Table 3). The change in melting endotherm peak temperature is possibly due to polymer-drug interactions, which are highest at higher Affinisol™ 15LV concentrations, resulting in a stronger melting point depression. The lack of a clearly distinguishable Tg in the 25 – 40 wt% compositions is likely due to overlapping thermal events. The observed melting endotherms for these compositions were particularly broad in appearance suggesting a broad range of melting point depression. It is therefore not possible within the bounds of this analysis to assign a specific polymorph.

At concentrations of 45 wt% and 50 wt% PCM a Tg re-appeared at 54.3 ˚C and 52. 5 ˚C, respectively, which are similar to the Tg values for the 5, 10 and 20 wt% formulations. Additionally, these compositions showed a much narrower, sharper melting endotherm. This may be indicative of a system composed of at least two phases, amorphous and crystalline. Baird and Taylor [35] reported that the crystallisation of the API in a solid dispersion can affect the measured Tg of the API-polymer system, since the concentration of polymer increases in the remaining amorphous phase. Interestingly, the mechanical properties and printability of extruded filaments match the presence (printable) and absence (not printable) of Tgs in these formulations (Figure 15, Table 3).

During the cooling cycle, all compositions showed a single Tg (Figure 15). Solanki et al. states that this is indicative of drug polymer miscibility [21]. With the exception of the highest (50 wt% PCM) mixture, no apparent fusion peaks were observed. In the case of the 50 wt%, this fusion peak is extremely small.

Tg depressions of polymers have previously been used to measure the plasticising effects of additives, since Tg is a function of chain mobility [36]. Here, the higher the drug loading the

lower the Tg with respect to the pure polymer. The Tg midpoint of Affinisol™ 15LV was 102.2˚C. The Tg of Affinisol™ 15LV has previously been determined by dielectric spectroscopy at 115˚C (Dow, Affinisol™ HPMC HME product information). The discrepancy between the two values can be attributed to the use of different techniques. With drug loadings increasing up to 20 wt%, substantial Tg depression was observed. With further increase in drug loading (between 25 – 50 wt%) the relative change of Tg decreases and were only slightly higher than the Tg of amorphous PCM.

In the 2nd heating cycle a clear trend of glass transition temperatures was observed similar to the cooling cycle. Amorphous PCM, had a Tg of 24.4˚C, followed by an exothermic cold crystallisation peak at 85.7˚C, a small exothermic cold crystallisation peak at 133˚C and a melting endotherm at 160˚C. Previous studies have attributed these exothermic peaks to form changes of PCM during the heating cycle. DSC-Raman and DSC-XRD studies attributed the exothermic peak at 85˚C as amorphous to form III crystallisation, the exothermic peak at 133˚C as transformation of form III to form II and the endothermic melting peak at 160˚C to the melt of form II [34, 37, 38]. The 50 wt% PCM formulation showed a cold crystallisation event at 135.1˚C. The following melting endotherm was observed at 160.4˚C suggesting that this may be form II. The differences in Tg observed between the first cooling cycle and the second heating cycle were likely to be because of the direction of heat transfer, i.e. upon cooling, the system is reaching lower temperatures to provide the driving force for Tg, hence observing slightly lower apparent Tg values. The aged samples show substantially different thermal behaviour. This is due to phase separation particularly at higher drug concentrations.

The thermogram of the freshly printed 50 wt% tablet (first heating cycle) was similar to the 2$^{nd}$ heating cycle of the aged filament seen as a low Tg (at ~ 25°C), an exotherm around 120-130°C, followed by a melting endotherm at 160°C (Figure 16 and Figure 17)

From this analysis, it is clear that by heating the 50 wt% filaments up to 190°C during the printing process the system was rendered largely amorphous at the point of printing. This was supported by the XRD data, the DSC data for the filaments and confirmed by the XRD and DSC data on freshly printed dose forms.

### *3.7 FFF 3D printing*

Four different tablet designs with variation on exposed surface area to volume were printed (Table 4). Tablets were printed using commercial PLA filament to enable a baseline physical comparison with tablets printed using filaments formulated at 10 wt% and 50 wt% PCM loadings from the present work. Examples of the 4 different designs printed across the three filament types are shown in Figure 3. Table 5 shows the details of the design and printed tablet dimensions and weights. The printer temperature used for the reported results was 190°C, from the DSC data the materials were fully liquefied at this temperature condition.

For all designs, the PLA filament generally resulted in dimensions slightly larger than the design dimensions in CAD. Based on the density of the PLA, all PLA printed tablets are typically

8-12 mg less than the design weight of 200 mg. This was because the design assumes perfectly flat surfaces and 100 % fill density but printing introduces some texture and porosity.

The 50 wt% PCM filament extruded readily at 190°C during the FFF printing process and showed extremely good tenacity of the polymer matrix to the print bed. Extrusion of the 50 wt% PCM filament resulted in dose forms with a slightly rough surface finish compared with the commercial PLA. Printed tablets were similar in dimensions to the PLA and again slightly larger than the CAD design dimensions. This is in part due to the similar reasons for the PLA but also due to the surface texture. Again, the CAD design assumes perfectly flat, smooth surfaces. The tablet weights were overall slightly closer to the target 200 mg than the PLA.

The 10 wt% filament did not extrude as readily at 190°C as the 50 wt% filament during the FFF printing process. During manual priming of the filament immediately before printing, greater resistance to flow was observed. Filament adhesion to the print bed for this formulation appeared to be poorer than the 50 wt%, i.e. upon printing the occasional dose form would release from the bed. This increased resistance during feeding the filament through the print nozzle is most likely due to the much higher viscosity of the 10 wt% formulation as there is less drug present to plasticise the polymer. Additionally, the higher viscosity and less fluid like nature of the 10 wt% formulation affects its tenacity and hence the ability to adhere to the bed. The printing unit used here did not have a heated bed which could help overcome this issue. Printed tablets were similar in dimensions to the PLA and again slightly larger than the CAD design dimensions. The tablet weights were significantly lower than the target weight and lower than PLA and the 50 wt%. This may be in part due to the presence of small bubbles in the 10 wt% filament (Figure 8) resulting in less material being deposited during the print process. The high melt viscosity and resistance to flow outlined above may result in some filament slippage in the extruder which in turn will influence the deposited weight.

It is evident from these findings, that further FFF process development is required for filaments with different melt rheologies in order to achieve target weights for a given formulation. However, this was beyond the aim of this study subsequent dissolution testing conducted normalised API dose based on final printed weights.

### *3.8 Content analysis of filaments.*

All filaments showed good agreement with the theoretical PCM content, with standard deviations between 0 and 0.7 % (Table 3). Only the 45 wt% formulation showed a slightly higher standard deviation of 1.9 %. Thus demonstrating that a homogeneous mixture was processed.

### *3.9 Drug Release studies*

Dissolution studies were carried out on freshly prepared 3DP tablets at sink conditions. All tablets released 100 % ± 5 % of the normalised API dose. Dose dumping was not observed. The relative standard deviation of drug release from 3DP tablet structures were between 3 %

and 10 %, with the lowest deviation for the SC tablet structure. The highest deviations were observed in the middle of the dissolution assay. All formulations, exhibited a slow release profile. This is likely to be due to release mechanisms in HPMC matrices generally following a polymer swelling mechanism [39]. Overall, API release was fastest for the largest surface area SLGE designs, which had open shallow channels, and slowest for the lowest surface area, SC design, which was a solid cylinder. The intermediate surface area SLG and SLGC designs lay between these. Release profiles ranged from > 80 % release at 1h 40 mins to 5h for the 10 wt% formulation and 6h for the 50 wt% formulation. The dissolution results for individual dose form designs for the 10 wt% and 50 wt% formulations are shown in Figure 18. Overlays of the 10 wt% and 50 wt% respectively are provided in supplementary data (Figure S 6 and Figure S 7).

For the two intermediate surface area designs (SLG and SLGC geometries), no significant difference was observed for the 10 wt% PCM formulation, since the standard deviation of both release curves overlapped. For the 50 wt% formulation the difference with respect to surface area is also modest. This may be due to the internal structure of these two designs being identical, i.e. the SLGC design was the SLG design internals with a thin outer cover.

These overall findings are in line with other reports identifying the surface area to volume ratio as one of the key variables controlling drug release from HPMC matrix tablets [39]. Similarly, Goyanes et al supported this finding, also showing that API release from 3DP dose forms was dependant on surface to volume ratio [40], however this was based purely upon external geometry and shape of the dose form rather than internal structure as is the case here.

The overall API dose did not affect the release profiles for the SLGE and SLG structures. For the SLGC and in particular, the SC dose forms, the higher 50 wt% API dose shows a slower release. It was observed that a gradual colour change from beige/clear to white occurred for the 50 wt% tablets during the dissolution assay. This indicates that the API is crystallising from the dose form. The SC being the slowest overall release may result in the greatest degree of precipitation and growth of the API as it has the longest contact time during the dissolution test, thus giving the greatest reduction in % released compared to the lower 10 wt% loading. The temperature increase during the dissolution assay with respect to the low Tg of the 50 wt% API-polymer matrix, the likelihood that the 50 wt% formulations are supersaturated in the amorphous state as well as hydration of the polymer increasing the molecular mobility in the system, would all contribute to crystallisation [41] of PCM. Crystallisation of API in ASD extrudates during dissolution has previously been described [42, 43]. Konno et al described a similar phenomenon for a 5 wt% and 50 wt% formulation of felodipine in povidone [42], where the dissolution rate of polymer and drug were similar in the low concentration formulation, but drug crystallisation occurred in the high concentration formulation during the dissolution assay. This is an important result which shows that development of a truly

wide ranging scalable dose form from 3DP technologies with tailored release based on dose form structure should be approached with care.

## 4 Conclusions

In this study, a viable operating space was developed and demonstrated to enable a novel pilot scale HME-Affinisol™ 15LV filament extrusion process suitable for FFF 3DP. This approach has not previously been reported and is the first commercially appropriate scale of HME for product development of 3DP dose forms via FFF (750 g/h and approximately 233 m/h filament equivalent to 60 doses per minute at 200 mg).

Using HME as a platform has demonstrated that substantial drug loadings for subsequent 3DP can be achieved. This level of API loading demonstrates that 3DP technology has the scope to achieve drug loadings that are equivalent to other well-established OSD manufacturing techniques such as wet granulation. It is also clear that it is possible to prepare and print filaments ranging from amorphous to suspended crystals. Additionally, at the point of printing, filaments with high drug loading solid suspensions are rendered back to the amorphous state.

From the development work carried out to control filament diameter across the range of API concentrations it is clear that optimisation is required to identify process conditions to compensate for composition dependant mixture properties in order to maintain suitable filament dimensions.

From the mechanical, DSC, XRD and 3D printer trials, across this wide range of drug loadings three basic types of extrudate were achieved. At 20 wt% API and below a printable filament, with a measurable Tg and sufficient flexural modulus was achieved. At API loadings between 25 and 35 wt% the filament could not be printed, had no measurable Tg and low flexural modulus. At higher drug loadings (~50 wt% API) the filaments had a Tg and a melting point, were printable and had sufficient flexural modulus. Therefore, when formulating filaments for FFF, there may only be selected compositions that will allow filaments with suitable dimensional and mechanical properties for FFF.

Utilising the mechanical testing method developed here appears to be a valuable low cost prediction tool for screening filaments and indication of suitability for the filament for FFF.

Within this work, once basic optimisation was achieved, die temperature could be used to compensate effects of increasing drug loading. From the dose forms printed and basic modification of the microstructure of 3D printed tablets, it was shown that substantial modifications to the release characteristics could be achieved for a fixed formulation composition.

For the 10 wt% API formulation the 80 % drug release point could be readily altered between 1h 40 mins to 5h and 6h 20 mins for the for the 50 wt% formulation. Overall, this work supports the findings of other workers that there are clear opportunities for FFF 3DP approaches for the development of simple, scalable and tuneable oral solid dose forms, but has highlighted some of the challenges met during process development at scale.

Conflict of Interest Statement:

There are no conflicts of interest with this work. All work contained in this manuscript is publicly funded academic work and there are no secondary interests associated with this manuscript.

All funding sources and contributors have been declared.

**Acknowledgement**

The authors would like to acknowledge that this work was carried out in the CMAC National Facility supported by UKRPIF (UK Research Partnership Fund) award from the Higher Education Funding Council for England (HEFCE) (Grant ref HH13054).

Funding from Advanced Manufacturing Supply Chain Initiative (AMSCI) for RE-configuring MEDIcines End-to-end Supply (REMEDIES) project (https://remediesproject.com/). We would like to thank GSK and AstraZeneca for their support in this project.

## 5 References

[1] S. Shah, M.A. Repka, Melt Extrusion in Drug Delivery: Three Decades of Progress, in: M.A. Repka, N. Langley, J. DiNunzio (Eds.), Melt Extrusion: Materials, Technology and Drug Product Design, Springer New York, New York, NY, 2013, pp. 3-46.
[2] M. Maniruzzaman, J.S. Boateng, M.J. Snowden, D. Douroumis, A Review of Hot-Melt Extrusion: Process Technology to Pharmaceutical Products, ISRN Pharmaceutics 2012 (2012) 9.
[3] M.R. Wilson, D.S. Jones, G.P. Andrews, The development of sustained release drug delivery platforms using melt-extruded cellulose-based polymer blends, The Journal of pharmacy and pharmacology 69(1) (2017) 32-42.

[4] D.G. Yu, L.-M. Zhu, C.J. Branford-White, X.L. Yang, Three-Dimensional Printing in Pharmaceutics: Promises and Problems, Journal of Pharmaceutical Sciences 97(9) (2008) 3666-3690.
[5] I.D. Ursan, L. Chiu, A. Pierce, Three-dimensional drug printing: A structured review, Journal of the American Pharmacists Association 53(2) (2013) 136-144.
[6] J. Goole, K. Amighi, 3D printing in pharmaceutics: A new tool for designing customized drug delivery systems, International Journal of Pharmaceutics 499(1) (2016) 376-394.
[7] L.K. Prasad, H. Smyth, 3D Printing technologies for drug delivery: a review, Drug Development and Industrial Pharmacy 42(7) (2016) 1019-1031.
[8] M.A. Alhnan, T.C. Okwuosa, M. Sadia, K.-W. Wan, W. Ahmed, B. Arafat, Emergence of 3D Printed Dosage Forms: Opportunities and Challenges, Pharmaceutical Research 33(8) (2016) 1817-1832.
[9] B.M.W. Giovanny F. Acosta-Velez, 3D Pharming: Direct Printing of Personalized Pharmaceutical Tablets, Polymer Science 2(1:3) (2016) 10.
[10] J. Norman, R.D. Madurawe, C.M.V. Moore, M.A. Khan, A. Khairuzzaman, A new chapter in pharmaceutical manufacturing: 3D-printed drug products, Advanced Drug Delivery Reviews 108 (2017) 39-50.
[11] A. Melocchi, F. Parietti, G. Loreti, A. Maroni, A. Gazzaniga, L. Zema, 3D printing by fused deposition modeling (FDM) of a swellable/erodible capsular device for oral pulsatile release of drugs, Journal of Drug Delivery Science and Technology 30, Part B (2015) 360-367.
[12] A. Goyanes, A.B.M. Buanz, A.W. Basit, S. Gaisford, Fused-filament 3D printing (3DP) for fabrication of tablets, International Journal of Pharmaceutics 476(1–2) (2014) 88-92.
[13] J. Skowyra, K. Pietrzak, M.A. Alhnan, Fabrication of extended-release patient-tailored prednisolone tablets via fused deposition modelling (FDM) 3D printing, European Journal of Pharmaceutical Sciences 68 (2015) 11-17.
[14] A. Goyanes, A.B.M. Buanz, G.B. Hatton, S. Gaisford, A.W. Basit, 3D printing of modified-release aminosalicylate (4-ASA and 5-ASA) tablets, European Journal of Pharmaceutics and Biopharmaceutics 89 (2015) 157-162.
[15] A. Goyanes, H. Chang, D. Sedough, G.B. Hatton, J. Wang, A. Buanz, S. Gaisford, A.W. Basit, Fabrication of controlled-release budesonide tablets via desktop (FDM) 3D printing, International Journal of Pharmaceutics 496(2) (2015) 414-420.
[16] T.C. Okwuosa, D. Stefaniak, B. Arafat, A. Isreb, K.-W. Wan, M.A. Alhnan, A Lower Temperature FDM 3D Printing for the Manufacture of Patient-Specific Immediate Release Tablets, Pharmaceutical Research 33(11) (2016) 2704-2712.
[17] A. Melocchi, F. Parietti, A. Maroni, A. Foppoli, A. Gazzaniga, L. Zema, Hot-melt extruded filaments based on pharmaceutical grade polymers for 3D printing by fused deposition modeling, International Journal of Pharmaceutics 509(1–2) (2016) 255-263.
[18] K. Pietrzak, A. Isreb, M.A. Alhnan, A flexible-dose dispenser for immediate and extended release 3D printed tablets, European Journal of Pharmaceutics and Biopharmaceutics 96 (2015) 380-387.
[19] J. Zhang, X. Feng, H. Patil, R.V. Tiwari, M.A. Repka, Coupling 3D printing with hot-melt extrusion to produce controlled-release tablets, Int J Pharm 519(1-2) (2017) 186-197.
[20] O.S. Carneiro, A.F. Silva, R. Gomes, Fused deposition modeling with polypropylene, Materials & Design 83 (2015) 768-776.
[21] N.G. Solanki, M. Tahsin, A.V. Shah, A.T.M. Serajuddin, Formulation of 3D Printed Tablet for Rapid Drug Release by Fused Deposition Modeling: Screening Polymers for Drug Release, Drug-Polymer Miscibility and Printability, J Pharm Sci 107(1) (2018) 390-401.

[22] M.T. Islam, J. Robertson, F. Tahir, A. Florence, Investigating processing window of Affinisol™ and Plasdone™ - S630 polymers during hot-melt extrusion (for 3D printing by fused deposition modelling), 7th APS International PharmSci Conference, Glasgow, United Kingdom, 2016.
[23] R.C. Bennett, J.M. Keen, Y. Bi, S. Porter, T. Dürig, J.W. McGinity, Investigation of the interactions of enteric and hydrophilic polymers to enhance dissolution of griseofulvin following hot melt extrusion processing, Journal of Pharmacy and Pharmacology 67(7) (2015) 918-938.
[24] S.S. Gupta, N. Solanki, A.T.M. Serajuddin, Investigation of Thermal and Viscoelastic Properties of Polymers Relevant to Hot Melt Extrusion, IV: Affinisol™ HPMC HME Polymers, AAPS PharmSciTech 17(1) (2016) 148-157.
[25] S. Huang, K.P. O'Donnell, J.M. Keen, M.A. Rickard, J.W. McGinity, R.O. Williams, A New Extrudable Form of Hypromellose: AFFINISOL™ HPMC HME, AAPS PharmSciTech 17(1) (2016) 106-119.
[26] T. Labs, Filament volume and length, 2018. https://www.toybuilderlabs.com/blogs/news/13053117-filament-volume-and-length. (Accessed January 2018).
[27] L. Jiannan, O. Sakae, I. Nicolas, S. John, G. Costas, K. Shingo, Understanding the Processing Window of Hypromellose Acetate Succinate for Hot-Melt Extrusion, Part I: Polymer Characterization and Hot-Melt Extrusion, Advances in Polymer Technology 37(1) (2018) 154-166.
[28] J. Aho, J.P. Boetker, S. Baldursdottir, J. Rantanen, Rheology as a tool for evaluation of melt processability of innovative dosage forms, International Journal of Pharmaceutics 494(2) (2015) 623-642.
[29] J. Aho, J.P. Botker, N. Genina, M. Edinger, L. Arnfast, J. Rantanen, Roadmap to 3D-Printed Oral Pharmaceutical Dosage Forms: Feedstock Filament Properties and Characterization for Fused Deposition Modeling, J Pharm Sci 108(1) (2019) 26-35.
[30] G. Verstraete, A. Samaro, W. Grymonpre, V. Vanhoorne, B. Van Snick, M.N. Boone, T. Hellemans, L. Van Hoorebeke, J.P. Remon, C. Vervaet, 3D printing of high drug loaded dosage forms using thermoplastic polyurethanes, Int J Pharm 536(1) (2017) 318-325.
[31] I.-C. Wang, M.-J. Lee, D.-Y. Seo, H.-E. Lee, Y. Choi, W.-S. Kim, C.-S. Kim, M.-Y. Jeong, G.J. Choi, Polymorph Transformation in Paracetamol Monitored by In-line NIR Spectroscopy During a Cooling Crystallization Process, AAPS PharmSciTech 12(2) (2011) 764-770.
[32] P. Piccinni, Y. Tian, A. McNaughton, J. Fraser, S. Brown, D.S. Jones, S. Li, G.P. Andrews, Solubility parameter-based screening methods for early-stage formulation development of itraconazole amorphous solid dispersions, The Journal of pharmacy and pharmacology 68(5) (2016) 705-20.
[33] A. Alhalaweh, A. Alzghoul, D. Mahlin, C.A.S. Bergstrom, Physical stability of drugs after storage above and below the glass transition temperature: Relationship to glass-forming ability, International Journal of Pharmaceutics 495(1) (2015) 312-317.
[34] R. Telford, C.C. Seaton, A. Clout, A. Buanz, S. Gaisford, G.R. Williams, T.J. Prior, C.H. Okoye, T. Munshi, I.J. Scowen, Stabilisation of metastable polymorphs: the case of paracetamol form III, Chem Commun (Camb) 52(81) (2016) 12028-12031.
[35] J.A. Baird, L.S. Taylor, Evaluation of amorphous solid dispersion properties using thermal analysis techniques, Adv Drug Deliv Rev 64(5) (2012) 396-421.

[36] Y. Li, H. Pang, Z. Guo, L. Lin, Y. Dong, G. Li, M. Lu, C. Wu, Interactions between drugs and polymers influencing hot melt extrusion, The Journal of pharmacy and pharmacology 66(2) (2014) 148-66.
[37] J.F. Kauffman, L.M. Batykefer, D.D. Tuschel, Raman detected differential scanning calorimetry of polymorphic transformations in acetaminophen, J Pharmaceut Biomed 48(5) (2008) 1310-1315.
[38] A. Rossi, A. Savioli, M. Bini, D. Capsoni, V. Massarotti, R. Bettini, A. Gazzaniga, M.E. Sangalli, F. Giordano, Solid-state characterization of paracetamol metastable polymorphs formed in binary mixtures with hydroxypropylmethylcellulose, Thermochim Acta 406(1-2) (2003) 55-67.
[39] T.D. Reynolds, S.A. Mitchell, K.M. Balwinski, Investigation of the effect of tablet surface area/volume on drug release from hydroxypropylmethylcellulose controlled-release matrix tablets, Drug Development and Industrial Pharmacy 28(4) (2002) 457-466.
[40] A. Goyanes, P.R. Martinez, A. Buanz, A.W. Basit, S. Gaisford, Effect of geometry on drug release from 3D printed tablets, International Journal of Pharmaceutics 494(2) (2015) 657-663.
[41] S. Baghel, H. Cathcart, N.J. O'Reilly, Polymeric Amorphous Solid Dispersions: A Review of Amorphization, Crystallization, Stabilization, Solid-State Characterization, and Aqueous Solubilization of Biopharmaceutical Classification System Class II Drugs, Journal of Pharmaceutical Sciences 105(9) (2016) 2527-2544.
[42] H. Konno, T. Handa, D.E. Alonzo, L.S. Taylor, Effect of polymer type on the dissolution profile of amorphous solid dispersions containing felodipine, Eur J Pharm Biopharm 70(2) (2008) 493-9.
[43] G.F.-D.d. Castillo, Dynamics and amorphous state stability of pharmaceuticals in hot melt extruded solid dispersions, Department of Applied Physics, Chalmers University of Technology, 2015, p. 110.

**List of Figures**:

Figure 12: a) Stress-strain graph of 3-point-bend flexural test of wt% PCM-Affinisol™ 15LV filaments and b) their associated flexural moduli (n = 5): Dark blue: 5 wt%, black 10 wt%, green 20 wt%, purple 25 wt%, pink 30 wt%, light blue 35 wt%, yellow 40 wt%, brown 45 wt%, red 50 wt% PCM-Affinisol™ 15LV.

Figure 13: XRD pattern for PCM, Affinisol™ 15LV and PCM-Affinisol™ 15LV a) physical mixtures and b) extruded (pelletised) filaments (5, 10, 20 and 50 wt% PCM).

Figure 14: XRD pattern of Paracetamol Powder, Affinisol™ 15LV, 3D printed tablet containing 5 wt%, 10 wt%, 20 wt% and 50 wt% Paracetamol within Affinisol™ 15LV HPMC matrices.

Figure 15: Glass transition temperatures of samples (n = 3) during DSC heating/cooling cycles. First heating cycle – green, Cooling cycle – red, second heating cycle – blue. Printable filaments indicated with *.

Figure 16: DSC thermogram of pelletised 50 wt% PCM-Affinisol™ 15LV formulation: red – 1st heating cycle, blue – cooling cycle, purple – 2nd heating cycle.

Figure 17: DSC thermogram of freshly printed 50 wt% PCM-Affinisol™ 15LV tablet: green - 1$^{st}$ heating cycle (0 - 190 °C), blue - cooling cycle (190 - 0 °C), pink – 2$^{nd}$ heating cycle (0 - 190 °C).

Figure 18: Comparison of in-vitro drug release profile 3DP tablet designs at 10 wt% and 50 wt% drug loading (n = 6). Tablet designs: a) SLGE – slotted grid extended, b) SLG – slotted grid, c) SLGC - slotted grid capped, d) SC – solid cylinder..

**List of Tables**



Table 1: Effect of feed rate and screw speed on Affinisol™ 15LV filaments diameter and torque measurements.

| Extruder Die Diameter (mm) | Screw Speed (rpm) | Feed Rate (kg/h) | Diameter of the filaments (Avg. ± SD) | Extruder Torque (Nm) (Avg. ± SD) | Pressure (Bar) (Avg. ± SD) |
|---|---|---|---|---|---|
| 1.5 | 200 | 1.0 | 1.89 ± 0.02 | 17.2 ± 0.6 | 40.1 ± 6.3 |
| | 100 | | NA | >24 | NA |
| | 200 | 0.75 | 1.89 ± 0.02 | 14.9 ± 1.8 | 33.2 ± 9.5 |
| | 150 | | 1.87 ± 0.02 | 16.9 ± 0.9 | 39.7 ± 4.4 |
| | 100 | | 1.81 ± 0.01 | 18.6 ± 1.4 | 45.8 ± 9.1 |
| | 50 | | 1.77 ± 0.02 | 21.0 ± 0.9 | 50.7 ± 4.6 |

Table 2: Effect of HME die zone temperature on the diameter of filaments of binary mixtures of PCM and Affinisol™ 15LV. (Processing conditions: barrel temperature zone 2 – 50 °C, zone 3 – 100 °C, zone 4 - 10 – 180 °C, screw speed 50 rpm, feed rate 0.75 kg/h).

| PCM / Affinisol™ 15LV (wt%) | HME Die Diameter (mm) | Die Zone Temperature (°C) | Diameter of the filaments (Avg. ± SD) (n = 10) |
|---|---|---|---|
| 5/95 | 1.5 | 180 | 1.68 ± 0.01 |
| | 1.6 | 180 | 1.76 ± 0.02 |
| | | 170 | 1.80 ± 0.01 |
| 10/90 | | 170 | 1.75 ± 0.03 |
| 20/80 | | 170 | Viscosity too low to support a strand |
| | | 160 | Viscosity too low to support a strand |
| | | 150 | 1.66 ± 0.02 |
| | | 140 | 1.76 ± 0.01 |
| 30/70 | | 140 | 1.71 ± 0.03 |
| | | 130 | 1.75 ± 0.03 |
| 40/60 | | 130 | 1.53 ± 0.04 |
| | | 120 | 1.67 ± 0.05 |
| | | 110 | 1.77 ± 0.03 |
| 50/50 | | 110 | 1.68 ± 0.02 |
| | | 100 | 1.75 ± 0.03 |

Table 3: PCM-Affinisol™ 15LV formulations (5 - 50 wt% PCM): Tg midpoint temperature and melting endotherm peak temperature in first DSC heating cycle, printability, average and standard deviation PCM content (wt%) (n=3) determined by UV analysis.

| Formulation | Tg midpoint (˚C), first heating cycle | Melting endotherm peak (˚C) | Printability | average wt% PCM content (n=3) | standard deviation |
|---|---|---|---|---|---|
| 5PCM | 54.6 | - | ✓ | 5.1 | 0.0 |
| 10PCM | 51.9 | - | ✓ | 9.9 | 0.0 |
| 20PCM | 48.6 | 139.7 | ✓ | 19.8 | 0.3 |
| 25PCM | - | 149.7 | × | 24.6 | 0.2 |
| 30PCM | - | 150.5 | × | 29.4 | 0.2 |
| 35PCM | - | 153.6 | × | 34.3 | 0.2 |
| 40PCM | - | 159.2 | × | 38.9 | 0.3 |
| 45PCM | 54.3 | 157.8 | ✓ | 44.5 | 1.9 |
| 50PCM | 52.5 | 160.3 | ✓ | 50.4 | 0.7 |
| PCM powder | - | 171-172 | × | n/a | n/a |

Table 4: Volume, Total surface area, outside surface area and specific surface area of 3DP tablet designs (figures calculated from SOLIDWORKS©).

| Design | Volume ($mm^3$) | Total surface area ($mm^2$) | Outside Surface Area ($mm^2$) | SAt/Vt ($mm^2/mm^3$) |
|---|---|---|---|---|
| Solid cylinder (SC) | 157.6 | 189.6 | 189.6 | 1.2 |
| Slotted grid with cap (SLGC) | 160.2 | 472.0 | 239.2 | 1.5 |
| Slotted grid (SLG) | 160.2 | 391.0 | 391.0 | 2.4 |
| Slotted grid extended (SLGE) | 155.3 | 515.1 | 515.1 | 3.3 |

Table 5: Tablet dimensions, average weights and standard deviation for different FFF printed tablet designs using PLA filament and the 10 wt% and 50 wt% PCM-Affinisol™ 15LV formulation compared to the Cura design file: Solid cylinder (SC), Slotted grid with cap (SLGC), slotted grid (SLG), slotted grid extended (SLGE extended).

| Filament | Design | diameter (mm) | height (mm) | length 1 (mm) | length 2 (mm) | average weight (mg) (n=3) | standard deviation |
|---|---|---|---|---|---|---|---|
| **Cura design** | SC | 8.00 | 3.20 | - | - | - | - |
| | SLGC | - | 2.80 | 8.00 | 9.00 | - | - |
| | SLG | - | 2.80 | 8.00 | 9.00 | - | - |
| | SLG extended | - | 1.40 | 9.00 | 16.00 | - | - |
| **PLA** | SC | 8.62 | 3.30 | - | - | 183.0 | 2.6 |
| | SLGC | - | 2.80 | 8.30 | 9.33 | 192.5 | 7.3 |
| | SLG | - | 2.83 | 8.25 | 9.34 | 188.4 | 2.3 |
| | SLG extended | - | 1.43 | 9.04 | 16.14 | 189.1 | 5.6 |
| **50% PCM** | SC | 8.15 | 3.40 | - | - | 188.9 | 4.4 |
| | SLGC | - | 3.21 | 8.22 | 9.24 | 195.4 | 1.0 |
| | SLG | - | 3.06 | 8.27 | 9.33 | 198.3 | 1.5 |
| | SLG extended | - | 1.55 | 9.25 | 16.11 | 198.3 | 1.5 |
| **10% PCM** | SC | 7.81 | 3.37 | - | - | 161.5 | 3.2 |
| | SLGC | - | 3.11 | 8.13 | 9.09 | 168.0 | 0.5 |
| | SLG | - | 2.96 | 8.10 | 9.04 | 167.1 | 3.6 |
| | SLG extended | - | 1.59 | 9.12 | 16.08 | 159.5 | 2.2 |

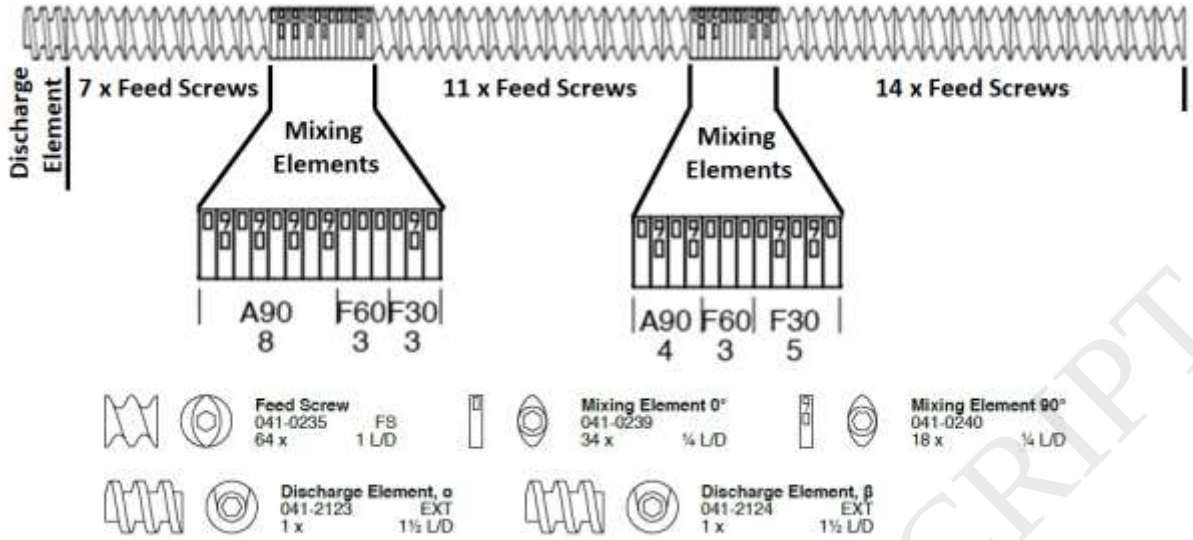


Figure 1: Screw configuration of the 16 mm extruder (HME Length (L)/Diameter (D) = 40 (40 × 16 mm = 640 mm) and screw elements used during this study (Conveying elements 1L/D, mixing elements ¼ L/D). Mixing element configuration: A90 = alternating mixing element types 0° and 90° at 90° to each other; F60 = mixing element type 0° forward at 60°; F30 = alternating mixing element types 0° and 90° forward at 30°.

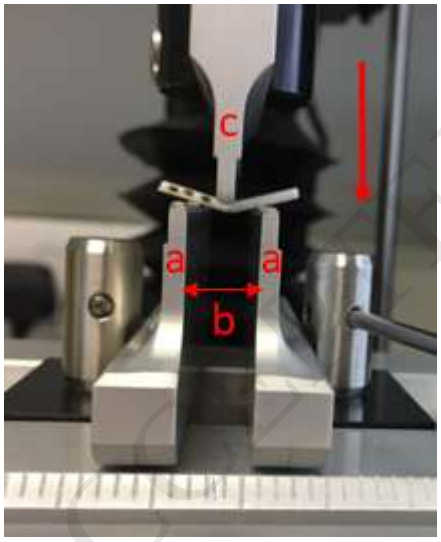


Figure 2: Flexural test setup: Texture Analyser TA-XT equipped with mini 3 point bend rig operated in compression mode (bold arrow indicating direction of test): a) lower support beams, b) gap (0.8cm), c) upper blade. A white test filament is mounted in the setup.

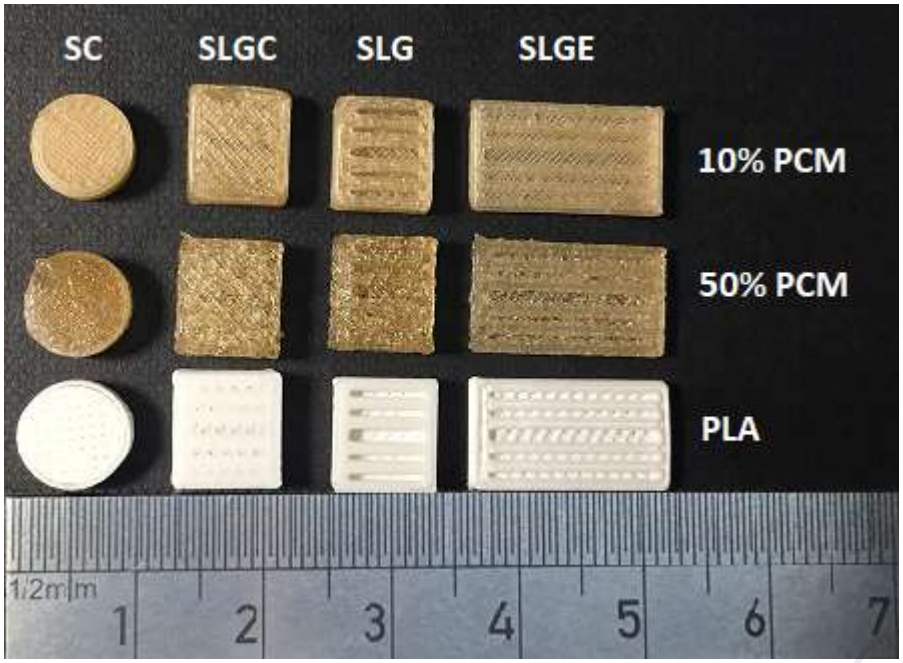


Figure 3: 3DP tablet shapes: SC – solid cylinder, SLGC – slotted grid with cap, SLG – slotted grid, SLGE – slotted grid extended; printed with PLA, 10 wt% PCM-Affinisol™ 15LV and 50 wt% PCM-Affinisol™ 15LV.

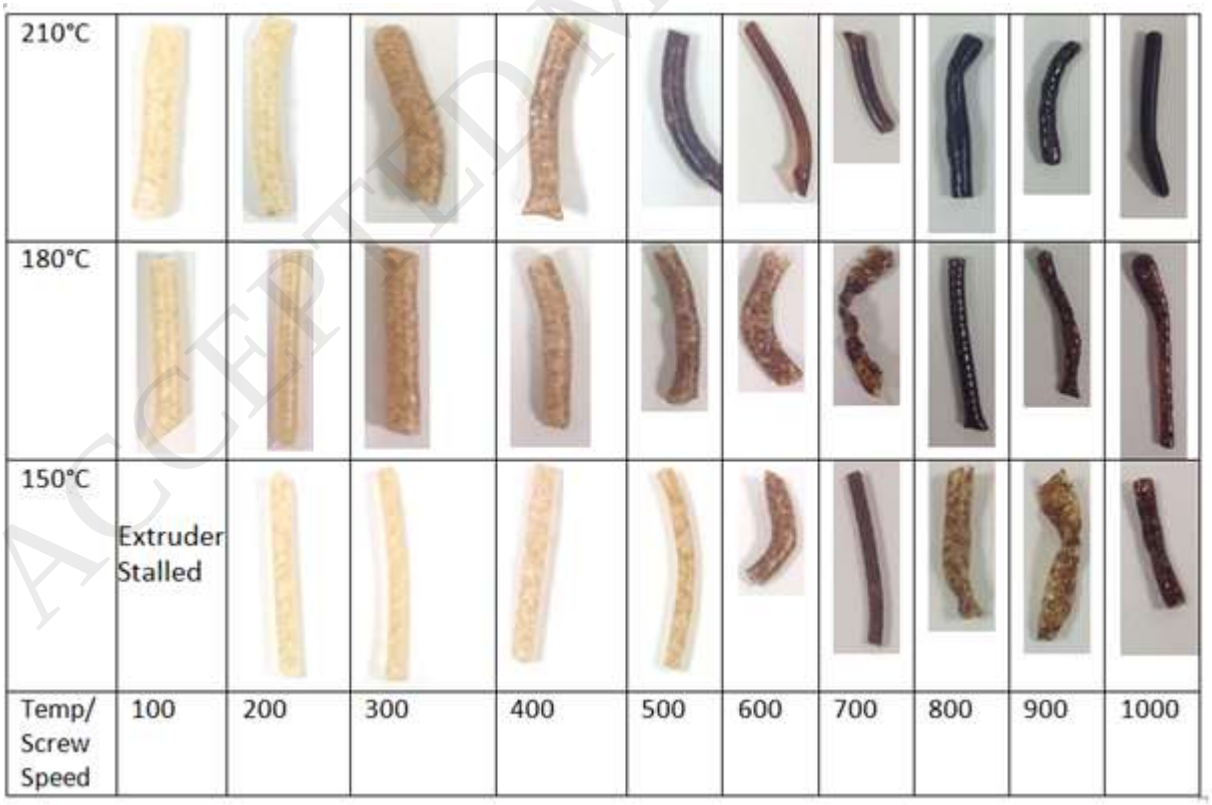

Figure 4: Images of filament samples from the HME screening of impact of operating conditions on Affinisol™ 15LV processed with the Eurolab 16.

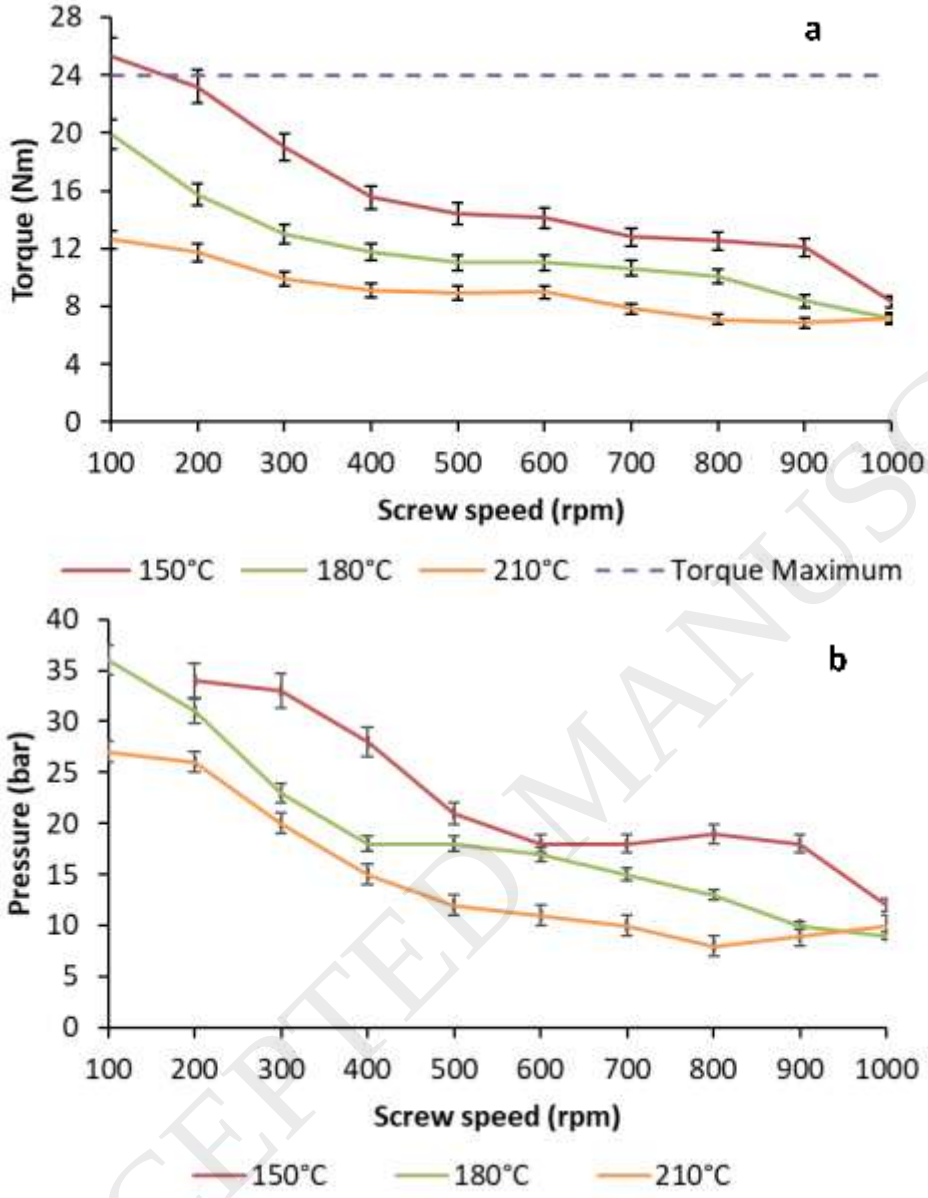


Figure 5: Effect screw speed on Torque (a) and Pressure (b) at 150°C, 180°C, 210°C processing temperature of Affinisol™ 15LV at 1 kg/h using a 3.0mm round die.

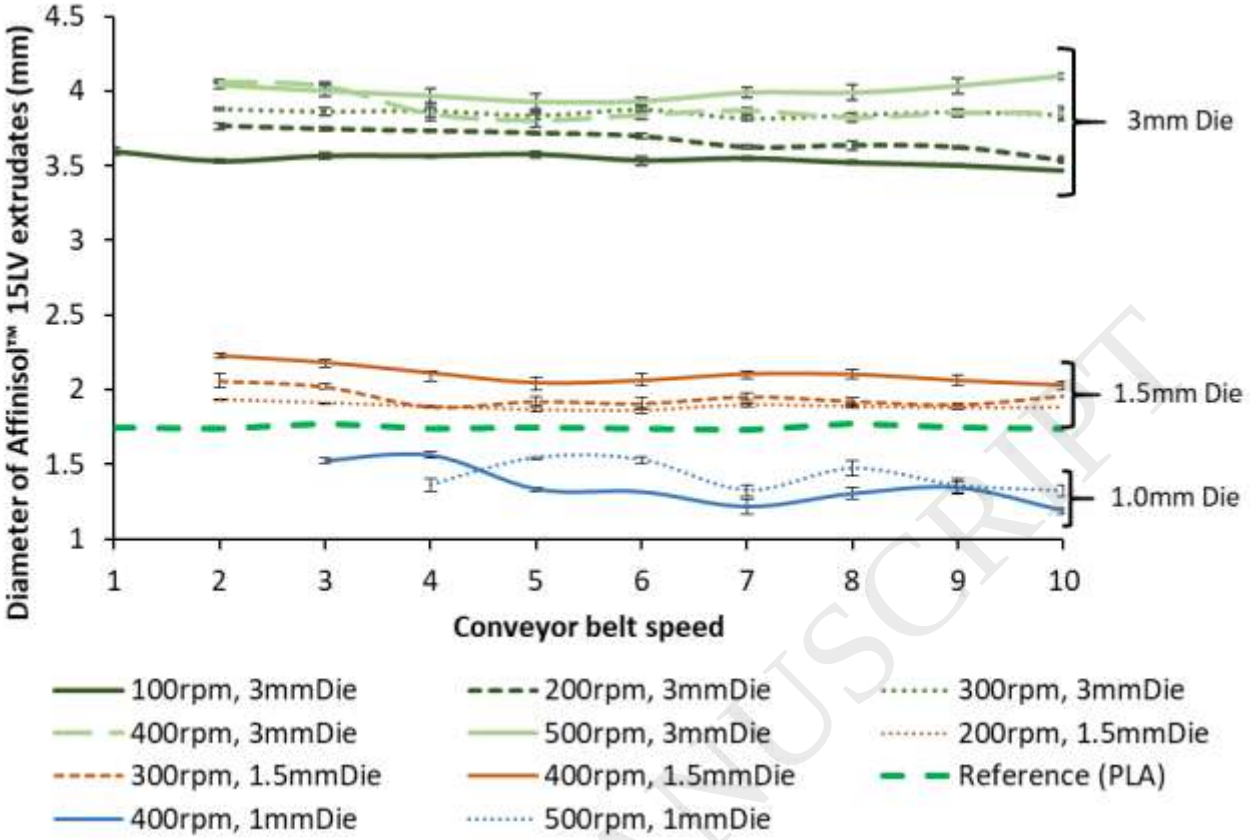


Figure 6: Diameter (mm) (n=10) of Affinisol™ 15LV filaments extruded at 1.0 kg/h feed rate, different screw speeds and extruded using 1.0, 1.5 and 3.0 mm extruder die exit. Reference target PLA filament (ex CEL ROBOX).

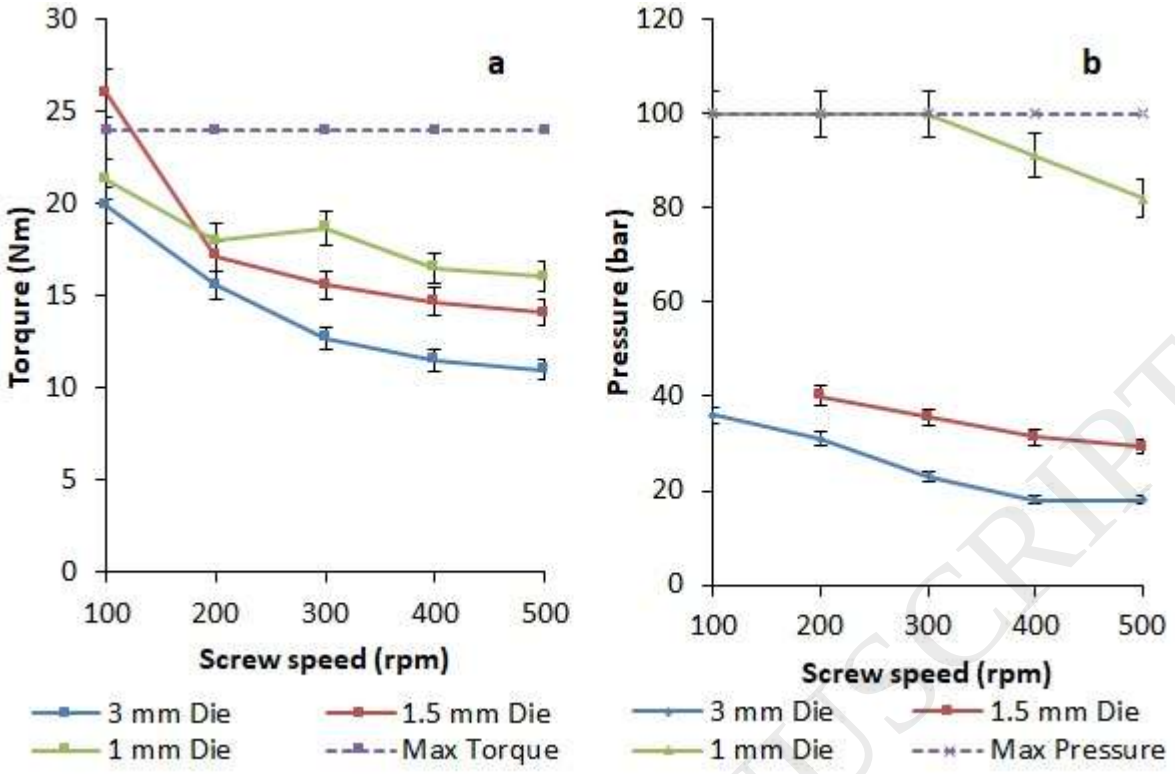


Figure 7: Effect of a) torque and b) pressure with increase in screw speed at 1.0, 1.5 and 3.0 mm extruder die exit (180 °C barrel temperature, 1 kg/h feed-rate).

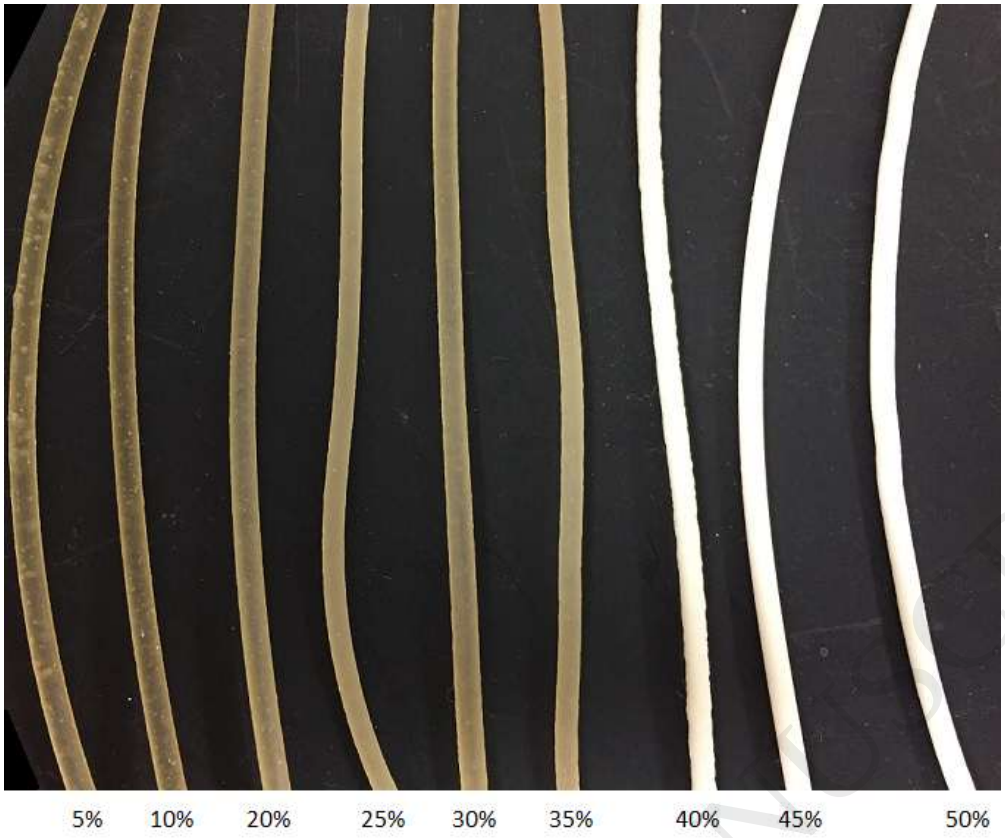


Figure 8: Extruded Affinisol™ 15LV filaments containing 5 – 50 wt% PCM.

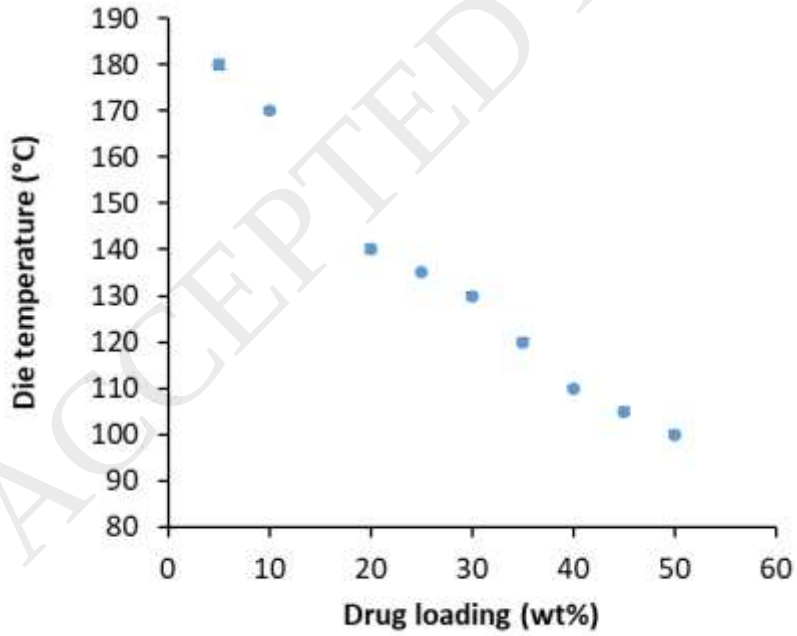


Figure 9: HME exit die temperature versus drug loading of Affinisol™ 15LV polymer.

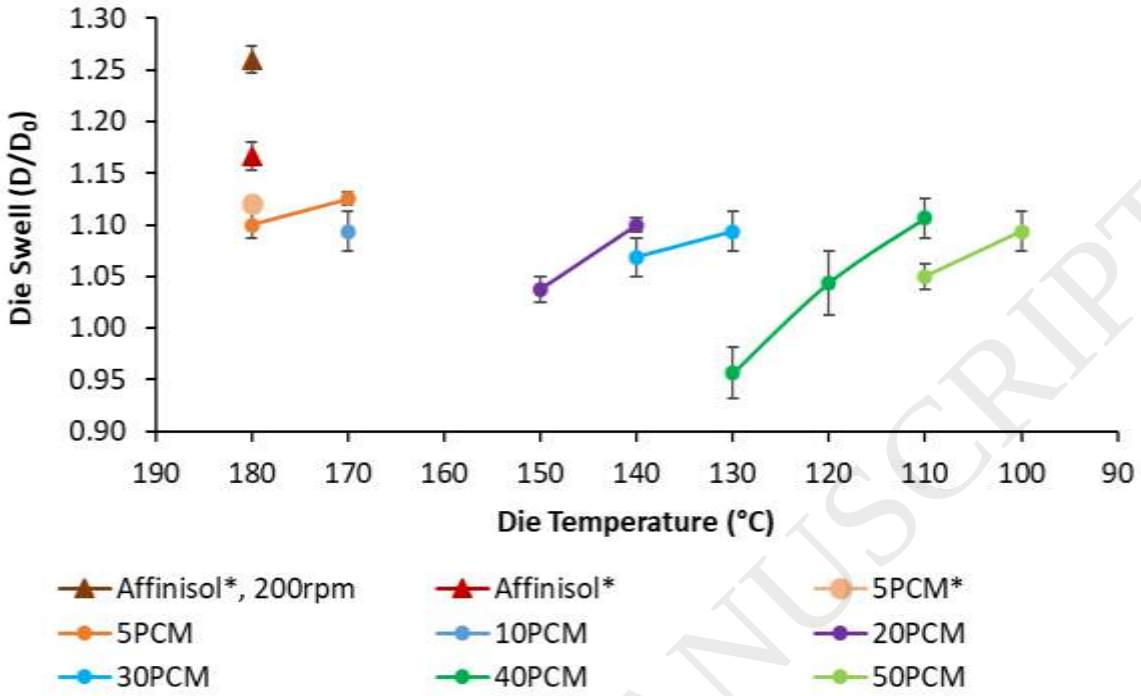


Figure 10: Die swell ratio of Affinisol™ 15LV and PCM-Affinisol™ 15LV formulations versus die Temperature extrusion with a 1.6 mm die at 180°C barrel temperature, 50 rpm screw speed and 0.75 kg/h feed rate (*1.5 mm die).

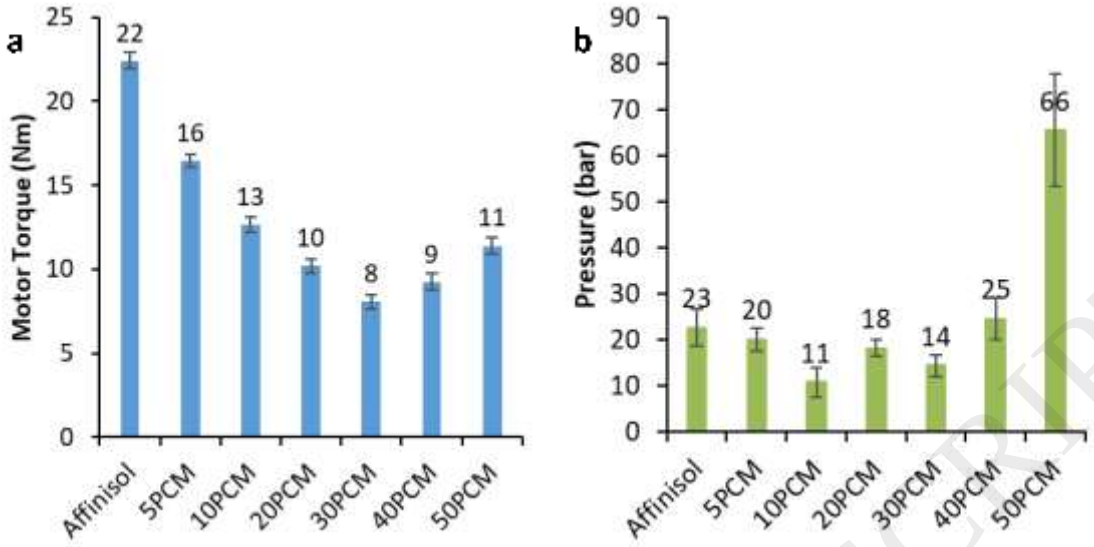


Figure 11: a) Motor toque values and b) associated pressure values for extrusion of filament strands with a 1.75 ± 0.5 mm diameter. Extrusion was performed with a feed rate of 0.75 kg/h at 180°C barrel temperature and a screw speed of 50rpm. Die temperatures were adjusted for PCM concentrations to maintain filament diameter: 5 wt% - 180°C, 10 wt% - 170°C, 20 wt% - 140°C, 30 wt% - 130°C, 40 wt% - 110°C, 50 wt% - 100°C.

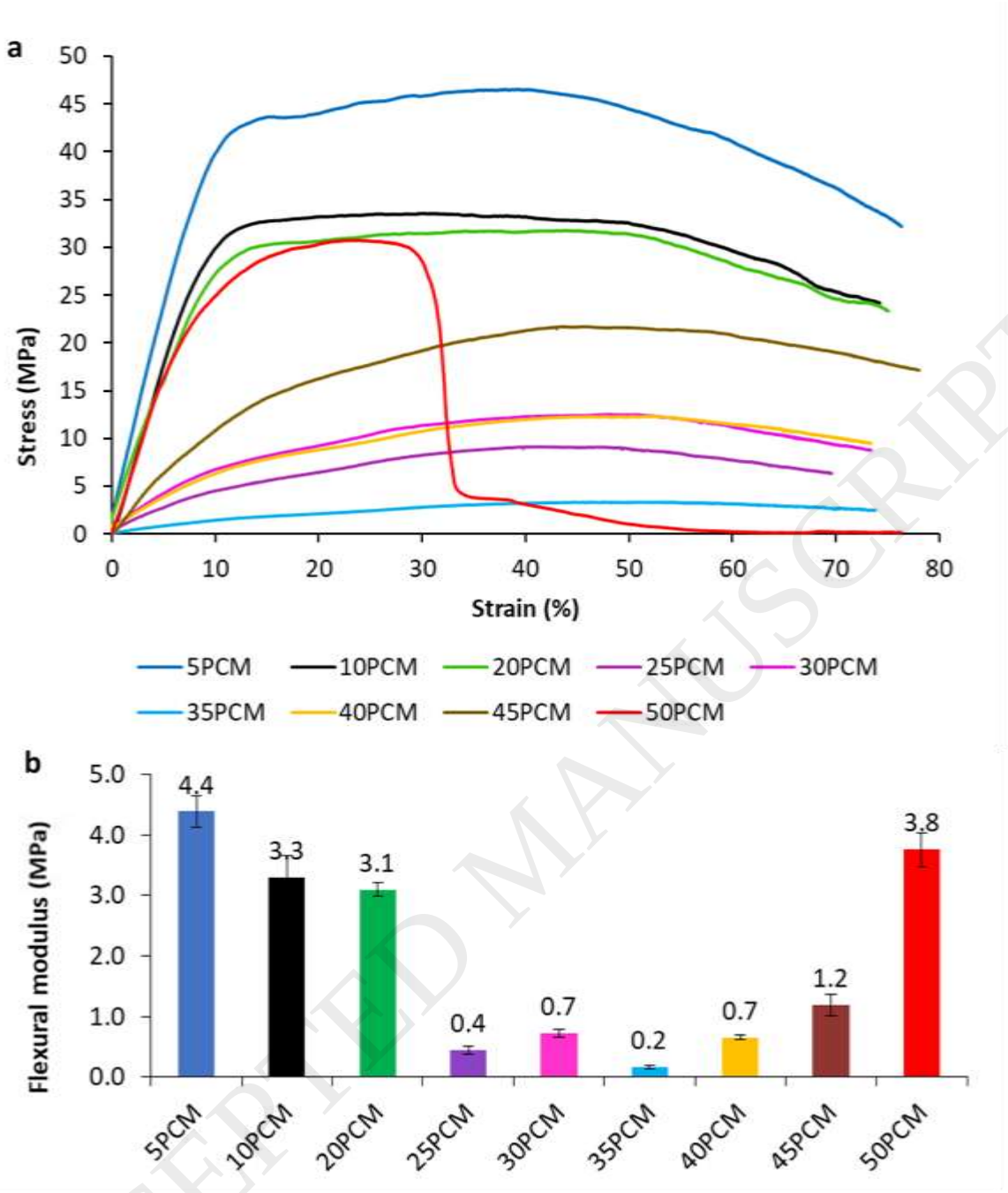


Figure 12: a) Stress-strain graph of 3-point-bend flexural test of wt% PCM-Affinisol™ 15LV filaments and b) their associated flexural moduli (n = 5): Dark blue: 5 wt%, black 10 wt%, green 20 wt%, purple 25 wt%, pink 30 wt%, light blue 35 wt%, yellow 40 wt%, brown 45 wt%, red 50 wt% PCM-Affinisol™ 15LV.

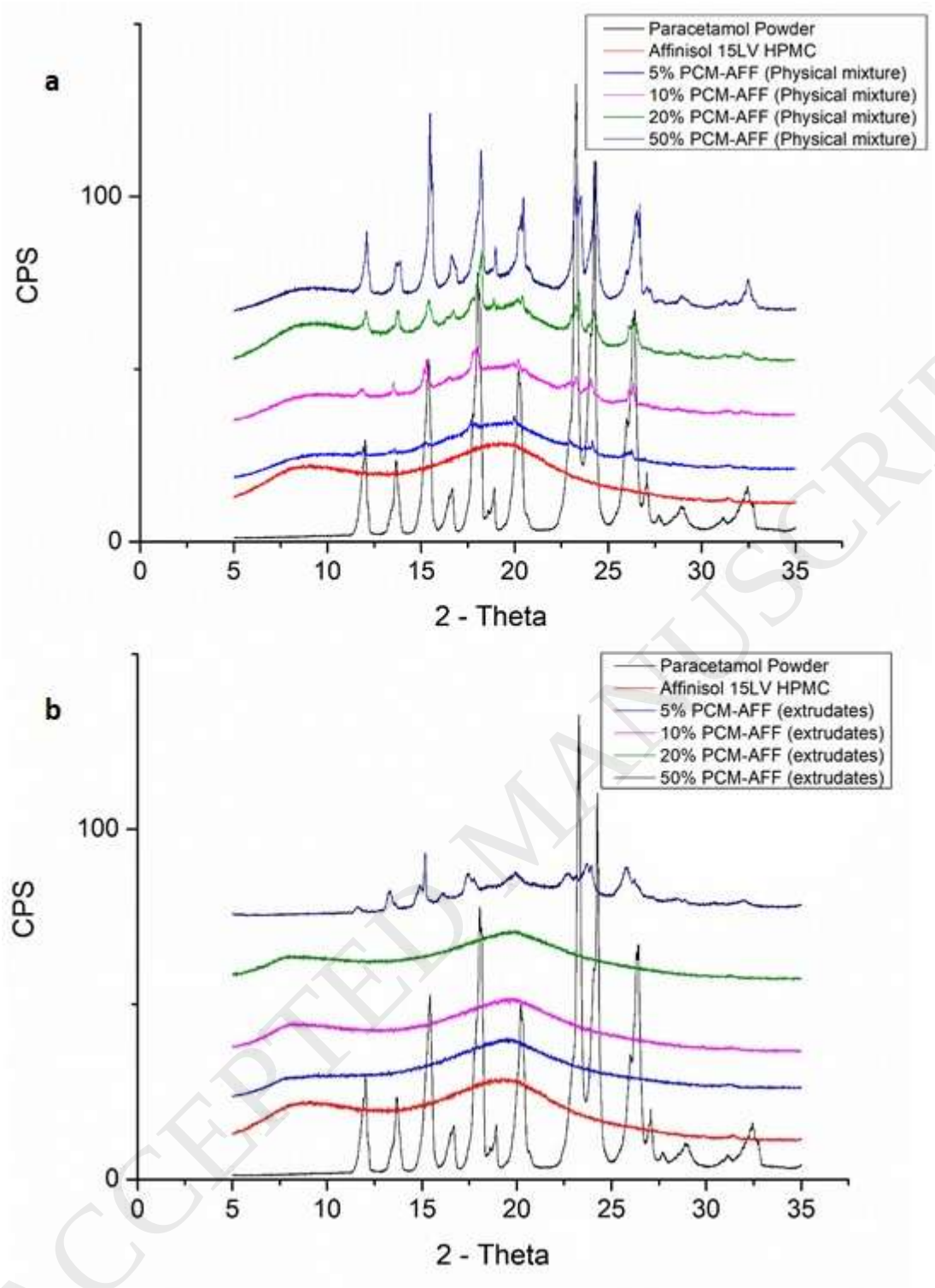


Figure 13: XRD pattern for PCM, Affinisol™ 15LV and PCM-Affinisol™ 15LV a) physical mixtures and b) extruded (pelletised) filaments (5, 10, 20 and 50 wt% PCM).

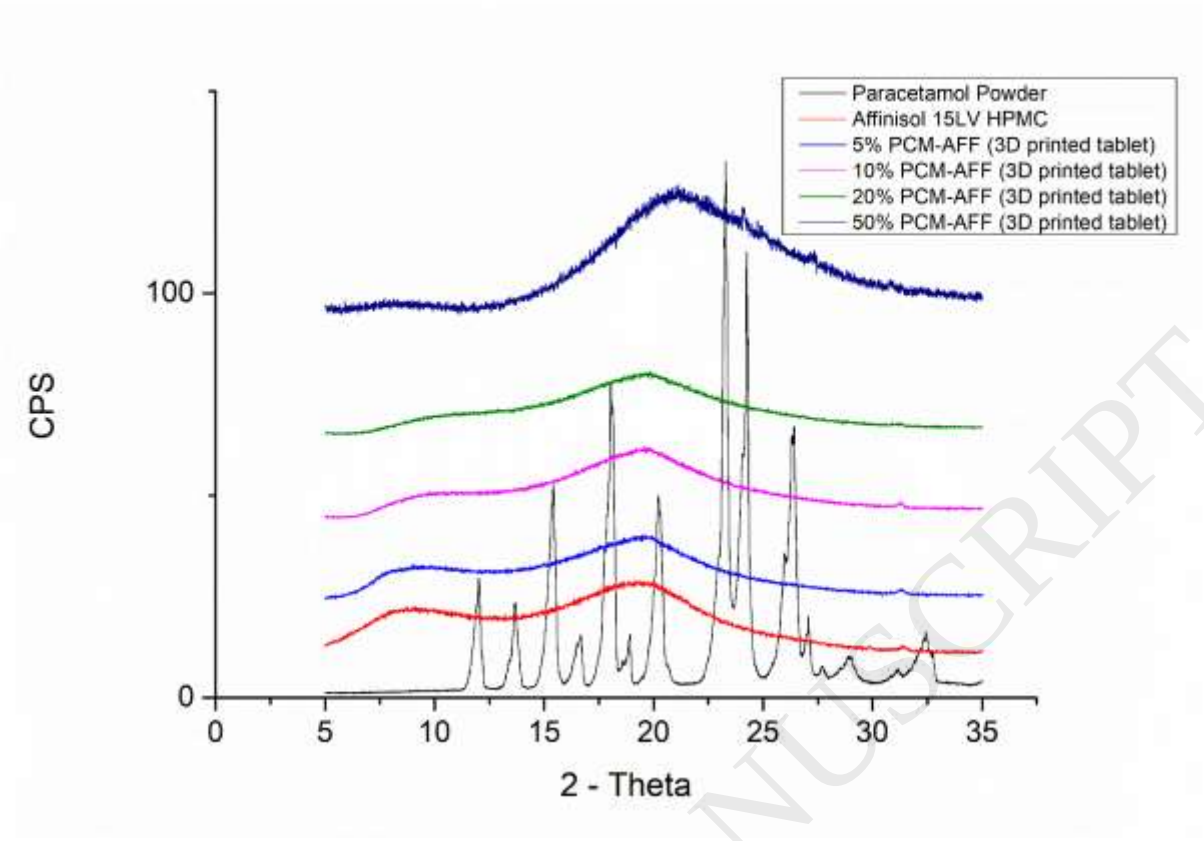


Figure 14: XRD pattern of Paracetamol Powder, Affinisol™ 15LV, 3D printed tablet containing 5 wt%, 10 wt%, 20 wt% and 50 wt% Paracetamol within Affinisol™ 15LV HPMC matrices.

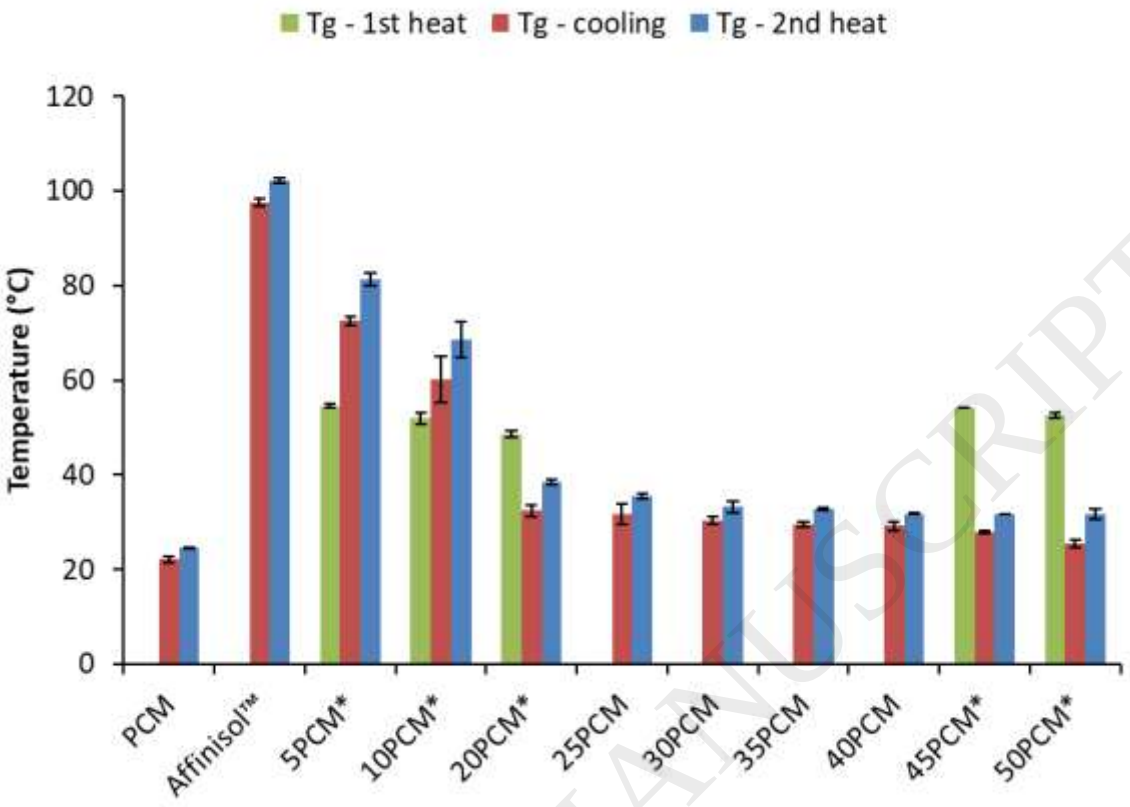


Figure 15: Glass transition temperatures of samples (n = 3) during DSC heating/cooling cycles. First heating cycle – green, Cooling cycle – red, second heating cycle – blue. Printable filaments indicated with *.

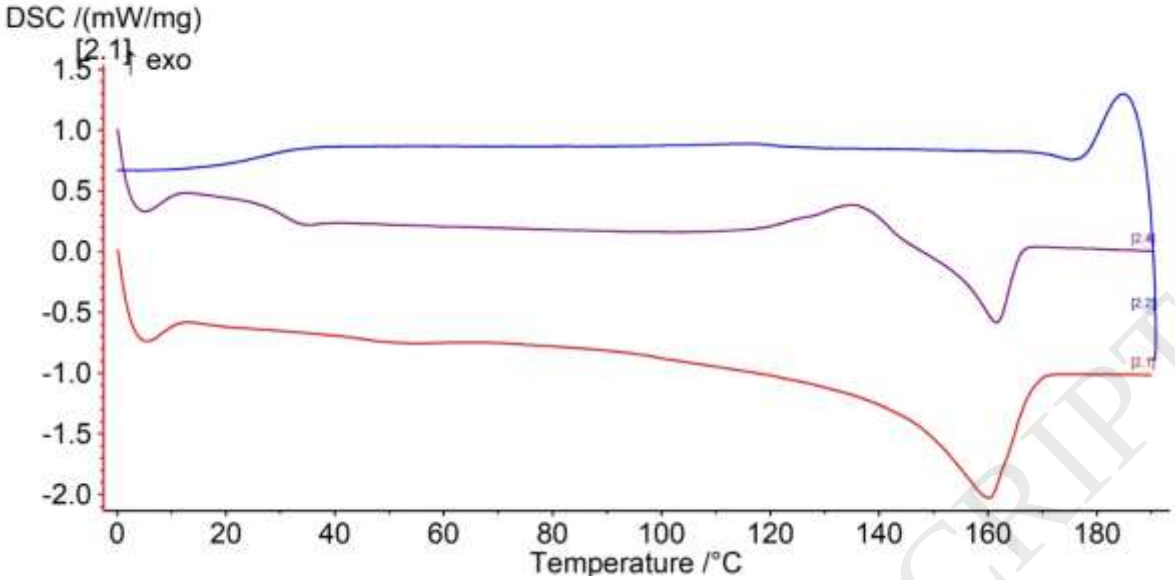


Figure 16: DSC thermogram of pelletised 50 wt% PCM-Affinisol™ 15LV formulation: red – 1st heating cycle, blue – cooling cycle, purple – 2nd heating cycle.

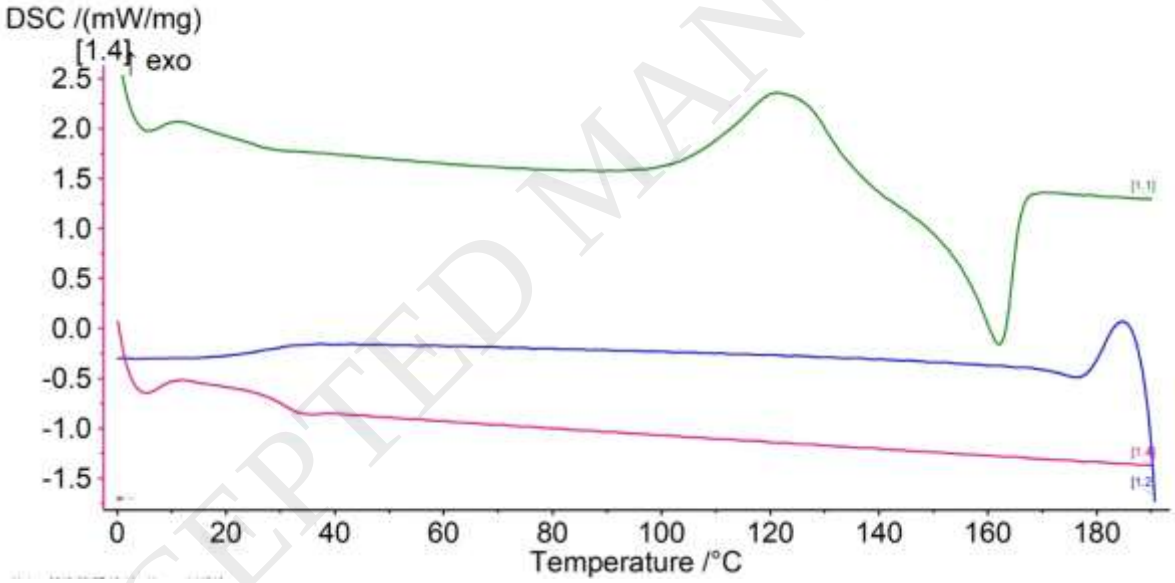


Figure 17: DSC thermogram of freshly printed 50 wt% PCM-Affinisol™ 15LV tablet: green - 1st heating cycle (0 - 190 °C), blue - cooling cycle (190 - 0 °C), pink – 2nd heating cycle (0 - 190 °C).

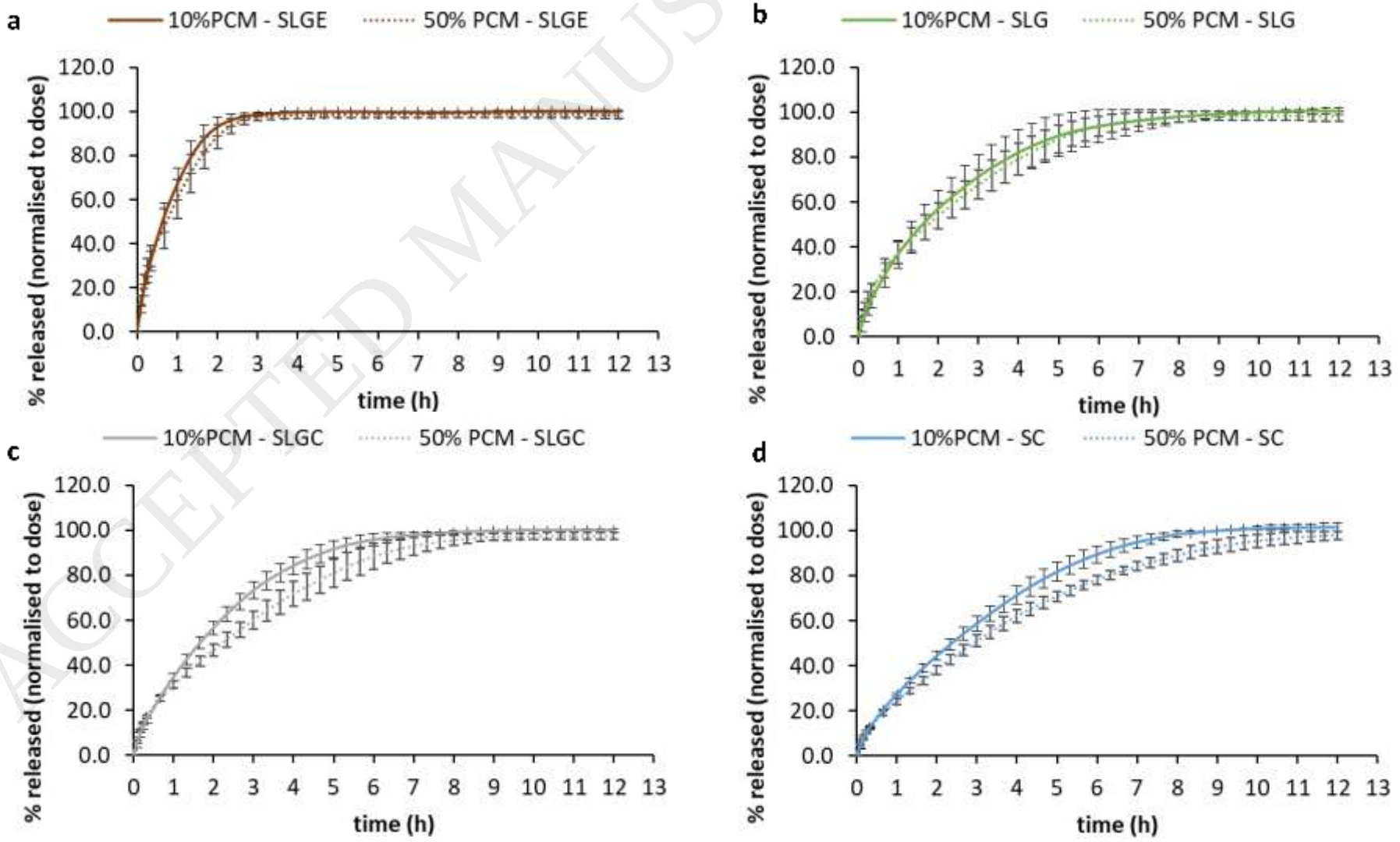

Figure 18: Comparison of in-vitro drug release profile 3DP tablet designs at 10 wt% and 50 wt% drug loading (n = 6). Tablet designs: a) SLGE – slotted grid extended, b) SLG – slotted grid, c) SLGC - slotted grid capped, d) SC – solid cylinder.

Table of Figures

Figure 15: Glass transition temperatures of samples (n = 3) during DSC heating/cooling cycles. First heating cycle – green, Cooling cycle – red, second heating cycle – blue. Printable filaments indicated with *.

Figure 16: DSC thermogram of pelletised 50 wt% PCM-Affinisol™ 15LV formulation: red – 1st heating cycle, blue – cooling cycle, purple – 2nd heating cycle.

Figure 17: DSC thermogram of freshly printed 50 wt% PCM-Affinisol™ 15LV tablet: green - 1st heating cycle (0 - 190 °C), blue - cooling cycle (190 - 0 °C), pink – 2nd heating cycle (0 - 190 °C).

Figure 18: Comparison of in-vitro drug release profile 3DP tablet designs at 10 wt% and 50 wt% drug loading (n = 6). Tablet designs: a) SLGE – slotted grid extended, b) SLG – slotted grid, c) SLGC - slotted grid capped, d) SC – solid cylinder.